Geosci. Model Dev. Discuss., https://doi.org/10.5194/gmd-2017-267
Manuscript under review for journal Geosci. Model Dev.
Discussion started: 1 December 2017

Geoscientific Model Development Discussions

Cohesive and mixed sediment in the Regional Ocean Modeling System (ROMS v3.6) implemented in the Coupled Ocean Atmosphere Wave Sediment-Transport Modeling System (COAWST r1179)

Christopher R. Sherwood[1], Alfredo L. Aretxabaleta[1], Courtney K. Harris[2], J. Paul Rinehimer[2,3], Romaric Verney[4], Bénédicte Ferré[1, 5]

[1]U. S. Geological Survey, 384 Woods Hole Road, Woods Hole, MA 02543-1598 USA
[2]Virginia Institute of Marine Sciences, Gloucester Point, Virginia, USA
[3]Currently at WEST Consultants, Bellevue, WA, USA
[4]IFREMER, Plouzane, France
[5]Currently at CAGE-Centre for Arctic Gas Hydrate, Environment, and Climate; Department of Geosciences, UiT The Arctic University of Norway, N-9037 Tromsø, Norway

Correspondence to: Christopher R. Sherwood (csherwood@usgs.gov)

Abstract. We describe and demonstrate algorithms for treating cohesive and mixed sediment that have been added to the Regional Ocean Modeling System (ROMS version 3.6), as implemented in the Coupled Ocean Atmosphere Wave Sediment-Transport Modeling System (COAWST Subversion repository revision 1179). These include: floc dynamics (aggregation and disaggregation in the water column); changes in floc characteristics in the seabed; erosion and deposition of cohesive and mixed (combination of cohesive and non-cohesive) sediment; and biodiffusive mixing of bed sediment. These routines supplement existing non-cohesive sediment modules, thereby increasing our ability to model fine-grained and mixed-sediment environments. Additionally, we describe changes to the sediment bed-layering scheme that improve the fidelity of the modeled stratigraphic record. Finally, we provide examples of these modules implemented in idealized test cases and a realistic application.

Geosci. Model Dev. Discuss., https://doi.org/10.5194/gmd-2017-267
Manuscript under review for journal Geosci. Model Dev.
Discussion started: 1 December 2017

1 Introduction

1.1 Motivation

Fine cohesive sediment (mud) is present in almost every coastal environment, and influences water clarity, benthic habitats, shoaling of harbors and channels, storage and transport of nutrients and contaminants, and morphologic evolution of wetlands, deltas, estuaries, and muddy continental shelves (Winterwerp and van Kesteren, 2004; Edmonds and Slingerland, 2010; Caldwell and Edmonds, 2014; Mehta, 2014; Li et al., 2017). The properties and behavior of mud depend on more than the size, shape, and density of the individual particles, so they are more difficult to characterize and model than properties of non-cohesive material like sand. Cohesive sediment often forms flocs that have lower densities, larger diameters, and faster settling velocities than the primary particles. Acoustic and optical sensors respond differently to suspensions of flocculated sediment, compared with similar mass concentrations of unflocculated particles, and these responses have important influences on observations of suspended-sediment mass concentrations, especially in estuaries (for example, McCave and Swift, 1976; McCave, 1984; Eisma, 1986; Hill and Nowell, 1995; Winterwerp, 1999, 2002; Winterwerp et al., 2006; Xu, Wang, and Riemer, 2008; 2010; Verney et al., 2011; Slade, Boss, and Russo, 2011; MacDonald et al., 2013; Thorne et al., 2014).

Cohesive sediment beds are distinguished by generally finer sediment, including some clay content, often are poorly sorted, and have low bulk density (high water content). Cohesive beds have a tendency for bulk responses to bottom stress, rather than individual particle responses. Cohesive beds have rheological properties that can range from fluids to Bingham plastics to granular materials, and may change with time in response to changes in water content, biochemical processes and fluid or geomechanical stresses (Dyer, 1986; Whitehouse et al., 2000; Winterwerp and Kranenburg, 2002; Winterwerp and van Kesteren, 2004; Maa et al., 2007; Knoch and Malcherek, 2011; Mehta, 2014).

Sediment transport in coastal ocean models is sensitive to the representation of fine-scale stratigraphy because evolving seabed properties determine what sediment is exposed to the water column and available for transport. Small-scale stratigraphy and grain-size distribution at the sediment-water interface also influence the grain roughness of the seabed, affect the type of small-scale roughness (biogenic features and ripples) present on the bed, and control properties like acoustic impedance of the seafloor. Biodiffusion influences stratigraphy by reducing gradients in grain size and other bed properties and by mixing materials from deeper in the bed to closer to the surface, where they may be more susceptible to transport.

Geosci. Model Dev. Discuss., https://doi.org/10.5194/gmd-2017-267
Manuscript under review for journal Geosci. Model Dev.
Discussion started: 1 December 2017

1.2 Previous Modeling Efforts

Amoudry and Souza (2011) surveyed regional-scale sediment-transport and morphology models, and found that one of the shortcomings was the treatment of cohesive- and mixed-sediment models. The water-column behavior of cohesive sediment (e.g., flocculation and disaggregation, and settling) and the consolidation of settling particles to form a cohesive bed has been modeled mostly with one-dimensional vertical (1DV) models or with empirical formulae that allow particle settling velocity to vary as a function of salinity (Ralston et al., 2012) or suspended-sediment concentration (e.g., Mehta, 1986; Lick et al., 1993; Van Leussen, 1994; Lumborg and Windelin, 2003; Lumborg, 2005; and Lumborg and Pejrup, 2005). The primary dynamical effect of flocculation is to increase settling velocities, thereby increasing the mass settling flux. Soulsby et al. (2013) reviewed methods for estimating floc settling velocities and proposed a new formulation that depends primarily on turbulence shear and instantaneous suspended-sediment concentration. Spearman et al. (2011) noted that adjustments to settling velocity (e.g., Manning and Dyer, 2007) were able to successfully reproduce floc settling in one-dimensional estuary modeling applications. However, these approaches do not allow analysis of other characteristics of the suspended particle field, such as acoustic and optical properties or geochemical properties (water content and surface area). Full floc dynamics have been incorporated in only a few coastal hydrodynamics and sediment-transport models. Winterwerp (2002) incorporated his floc model (Winterwerp, 1999) in a three-dimensional simulation of the estuary turbidity maximum (ETM) in the Ems estuary. Ditschke and Markofsky (2008) described formulations in TELEMAC-3D to represent exchanges among size classes from floc dynamics. Xu et al. (2010) added floc dynamics to the Princeton Ocean Model (POM) and simulated the ETM in Chesapeake Bay.

Empirical formulae for the erosion of cohesive sediment have been derived from laboratory flume measurements and field experiments (Whitehouse et al, 2000; Mehta, 2014). Many have a form similar to the Ariathurai and Arulanandan (1978) equation used in ROMS (Warner et. al., 2008), which relates erosional flux E (kg m^{-2} s^{-1}) to the normalized excess shear stress as $E = E_0(1-\phi)\left[(\tau_{sf} - \tau_c)/\tau_{sf}\right]$ when $\tau_{sf} > \tau_c$, and where E_0 (kg m^{-2} s^{-1}) is an empirical rate constant, ϕ (m^3/m^3) is sediment porosity, τ_{sf} (Pa) is the skin-friction component of the bottom shear stress, and τ_c (Pa) is the critical shear stress for erosion. Erosion of cohesive sediment in some models (for example Delft3D; van der Wegen et al., 2011; Caldwell and Edmonds, 2014) uses a similar formulation, subject to a user-specified critical shear stress for erosion. It is recognized that that τ_c may increase with depth in sediment, and erosion-rate formulae have been proposed that incorporate depth-dependent profiles for E_0 and/or τ_c (Whitehouse et al, 2000; Mehta, 2014). Wiberg et al. (1994) demonstrated the need to account for small-scale stratigraphy to represent bed armoring for a non-cohesive model, and did so via a layered bed model that kept track of changes to sediment-bed grain-size distribution in response to cycles of erosion and deposition. Bed layers have been used to represent temporal changes to bed erodibility for fine-grained sediment, for example by using an age model for the bed (HydroQual, 2004). Biodiffusion may alter stratigraphy, and there are many 1DV models that treat

diffusive mass flux of sediment and reactive constituents in the bed, mostly motivated by water-quality and geochemical concerns (e.g., Boudreau, 1997; DiToro, 2001; Winterwerp and van Kesteren, 2004). Several regional-scale circulation and sediment-transport models treat sediment stratigraphy, including ECOMSED (HydroQual, 2004), ROMS/CSTMS (Warner et al., 2008), Delft3D (van der Wegen et al., 2011), FVCOM, TELEMAC/SISYPHE (Villaret et al., 2007; Tassi and Villaret, 2014), and some have unpublished treatments for cohesive processes. Sanford (2008) pioneered an approach where the critical shear stress for each bed layer was nudged toward an assumed equilibrium value, and the critical stress for erosion of the surface layer alternately became smaller or larger in response to deposition and erosion. We have combined the approach of Sanford et al. (2008) with biodiffusive mixing to represent depth-dependent changes in erodibility. This approach has been implemented in the cohesive bed stratigraphy algorithm in ROMS (described here) and applied by Rinehimer et al. (2008), Butman et al. (2014), and Fall et al. (2014).

1.3 Goals of the Model

Our goal in developing and refining sediment dynamics in ROMS is to produce an open-source community model framework useful for research and management that combines cohesive and non-cohesive behavior and is suitable for simulating sediment transport, stratigraphic evolution, and morphologic change. Our goal is to develop methods that can be implemented within coastal and estuarine models for application at regional scales, i.e. domains of 10s to 100s of km^2 with grid elements of 10 – 10,000 m^2 and the ability to resolve time scales ranging from minutes to decades.

1.4 Objectives and Outline of the Paper

The behavior of non-cohesive sediment (sand) in ROMS was described by Warner et al. (2008). ROMS also includes several biogeochemical modules (Fasham et al., 1990; Fennel et al., 2006). New components have since been added, including spectral irradiance and seagrass growth model (del Barrio et al., 2014) and a model for treating the effects of submerged aquatic vegetation on waves and currents (Beudin et al., 2017). The present paper describes new components that model processes associated with cohesive sediment (mud) and mixtures of sand and mud. These include aggregation and disaggregation of flocs in the water column, sediment exchange with a cohesive bed where erosion is limited by a bulk critical shear stress parameter that increases with burial depth, and tracking stratigraphic changes in response to deposition, erosion, and biodiffusive mixing. Our goal is to demonstrate that the algorithms reproduce some of the important behaviors that distinguish cohesive sedimentary environments from sandy ones, and to demonstrate their utility for modeling muddy environments. The model processes are presented and discussed in Section 2. Additional details of the model implementation and their use in ROMS are presented in the Supplement. Examples of model behavior are presented in Section 3, and a realistic application in the York River Estuary is presented in Section 4. Discussion and Conclusions are in Sections 5 and 6.

Geosci. Model Dev. Discuss., https://doi.org/10.5194/gmd-2017-267
Manuscript under review for journal Geosci. Model Dev.
Discussion started: 1 December 2017

2 Model Processes

Flocculation is represented as a local process of aggregation and disaggregation that moves mass among the floc classes within each model grid cell during a ROMS baroclinic time step. ROMS uses a split time step scheme that integrates over several (ca. 20) depth-averaged (barotropic) time steps before the depth-dependent baroclinic equations are integrated (Shchepetkin and McWilliams, 2005). Subsequent advection and mixing of floc particles is performed along with other tracers (heat, salt, sand, biogeochemical constituents). The water column is coupled with the sediment bed via depositional fluxes determined by near-bed concentrations, settling velocities, and threshold shear stresses; and via erosional fluxes determined by bottom shear stresses, bulk and particle critical shear stresses for erosion, and sediment availability in the top, active layer (Warner et al., 2008). The distribution of mass among the cohesive classes can change in the bed as flocs are converted to denser aggregates. Deposition and erosion affect the mass of sediment classes in the stratigraphic record, which can also be changed by biodiffusive mixing and a heuristic model of erodibility as a function of time and sediment depth. Each of these processes is described below.

2.1 Properties of Sediment, Seafloor, and Seabed

ROMS accounts for two distinct types of sediment: non-cohesive sediment (e.g., sand) and cohesive sediment (e.g., mud). The general framework used to represent sediment and the seabed is unchanged from Warner et al. (2008), except that the expanded model requires additional variables to allow for both cohesive and non-cohesive classes. The number of sediment classes is presently limited to twenty-two of each type by the input/output formats, but is otherwise only constrained by computational resources. Each class must be classified as either non-cohesive or cohesive, and at least one class of one type is required for sediment-transport modeling. Each class is associated with properties (diameter, density, critical shear stresses for erosion and deposition, settling velocity) that are specified as input and remain constant throughout the model calculations. Seafloor properties that describe the condition of the sediment surface are stored with spatial dimensions that correspond to the horizontal model domain. Seafloor properties include representative values (geometric means) of sediment properties in the top layer, including grain size, critical shear stress for erosion, settling velocity, and density; and properties of the sediment surface, such as ripple height, ripple wavelength, and bottom roughness. Seabed properties (i.e. stratigraphy) are tracked at each horizontal location and in each layer in the bed. The number of layers used to represent seabed properties is specified as input and remains constant throughout the model run. The mass of each sediment class, bulk porosity, and average sediment age is stored for each bed layer. The layer thickness, which is calculated from porosity and the mass and sediment density for each class is stored for convenience, as is the depth to the bottom of each layer. Additional information for bulk critical shear stress is stored if the cohesive sediment formulation is being used.

Geosci. Model Dev. Discuss., https://doi.org/10.5194/gmd-2017-267
Manuscript under review for journal Geosci. Model Dev.
Discussion started: 1 December 2017

2.2 Floc Model

We implemented the floc model FLOCMOD (Verney et al., 2011) in ROMS to model changes in settling velocity and particle size caused by aggregation and disaggregation. Flocculation is represented as a local process that moves mass among the floc classes within each model grid cell during a ROMS baroclinic time step. Subsequent advection and mixing of floc particles is performed along with other tracers (heat, salt, sand, biogeochemical constituents). FLOCMOD is a population model (Smoluchowski, 1917) based on a finite number of size classes with representative floc diameters D_f (m). The model requires a relationship between floc size and floc density ρ_f (kg/m^3) that is related to the primary disaggregated particle diameter D_p (m) and density ρ_s (kg/m^3) through a fractal dimension n_f (dimensionless; Kranenburg, 1994) according to

$$\rho_f = \rho_w + (\rho_s - \rho_w)\left(\frac{D_f}{D_p}\right)^{n_f - 3} \quad (1)$$

where ρ_w (kg/m^3) is the density of the interstitial water in the flocs. The fractal dimension for natural flocs is typically close to 2.1 (Tambo and Watanabe, 1979; Kranenburg, 1994). Floc densities increase as n_f increases, and at n_f = 3, the flocs are solid particles with $\rho_f = \rho_s$. All cohesive sediment classes are treated as flocs when the floc model is invoked, and the processes of aggregation and disaggregation can shift mass of suspended sediment from one class to another. The floc model is formulated as a Lagrangian process that takes place within a model cell over a baroclinic model time step while conserving suspended mass in that cell, similar to the way that reaction terms are included in biogeochemical models (for example, Fennel et al., 2006). FLOCMOD simulates aggregation from two-particle collisions caused by either shear or differential settling, and disaggregation caused by turbulence shear and/or collisions. The rate of change in the number concentration $N(k)$ (m^{-3}) of particles in the k^{th} floc class is controlled by a coupled set of k of differential equations

$$\frac{dN(k)}{dt} = G_a(k) + G_{bs}(k) + G_{bc}(k) - L_a(k) - L_{bs}(k) - L_{bc}(k) \quad (2)$$

where G and L terms (m^{-3}s^{-1}) represent gain and loss of mass by the three processes denoted by subscripts: a (aggregation), bs (breakup caused by shear), and bc (breakup caused by collisions). Equations 2 are integrated explicitly using adjustable time steps that may be as long as the baroclinic model time step, but are decreased automatically when necessary to ensure stability and maintain positive particle number concentrations. Particle number concentrations $N(k)$ are related to suspended mass concentrations $C_m(k)$ (kg/m^3) via the volume and density of individual flocs. The aggregation and disaggregation terms (Verney et al., 2011) both depend on local rates of turbulence shear, which are calculated from the turbulence submodel in ROMS. Details of these processes are described in the Supplement.

The floc model introduces several parameters (see Supplement), some of which have been evaluated by Verney et al. (2011). These parameters are specified by the user. The equilibrium floc size depends on the ratio of aggregation to breakup parameters, and the rate of floc formation and destruction depends on their magnitudes (Winterwerp, 1999; 2002). The diameter, settling velocity, density, critical stress for erosion, and critical stress for deposition (described below) are required inputs for each sediment class, both cohesive and non-cohesive (see Supplement). The present implementation requires a fractal relationship between floc diameter and floc density (Kranenburg, 1994), and we have assumed a Stokes settling velocity. Alternative relationships between diameter and settling velocity, such as modified Stokes formula (e.g., Winterwerp, 2002; Winterwerp et al., 2002; Winterwerp et al., 2007; Droppo et al., 2005; Khelifa and Hill, 2006), could be used by adjusting input parameters, but alternative relationships between diameter and floc density (Khelifa and Hill, 2006; Nguyen and Chua, 2011) would require changes to the aggregation and disaggregation terms in FLOCMOD.

2.2.1. Fluxes into the bed – Critical shear stress for deposition

The settling flux of flocs (and all other size classes) into the bed (deposition) over a time step is calculated as $w_{s,k}\rho_k C_{v,k}\Delta t$ (kg m^{-2}, where $w_{s,k}$ (m/s), ρ_k (kg/m^3), and $C_{v,k}$ (m^3/m^3) are settling velocities, floc (or particle) densities, and volume concentrations for the kth size class in the bottom-most water-column layer, respectively, and Δt (s) is the baroclinic time step. An optional critical shear stress for deposition (τ_d; Pa; Krone, 1962; Whitehouse et al., 2000; Mehta, 2014) has been implemented for cohesive sediment. Deposition in our model is zero when the bottom stress τ_b (Pa) is greater than τ_d. When τ_b is less than τ_d, deposition increases linearly as τ_b decreases toward zero, behavior we call linear depositional flux (Whitehouse et al., 2000; see Supplement). A simpler alternative is to assume a full settling flux when $\tau_b < \tau_d$, which we call constant depositional flux, and which we have implemented as an option. According to Whitehouse et al. (2000), τ_d is typically about half the magnitude of the critical shear stress for erosion τ_c, but is unrelated to that value. Mehta (2014, Equation 9.83) suggested a relationship between τ_d for larger particles, using τ_d values for the smallest particles in suspension and the ratio of diameters raised to an exponent that depends on sediment properties (see Supplement), citing Letter (2009) and Letter and Mehta (2011). The effect of a critical shear stress for deposition is to keep sediment in suspension in the bottom layer. This results in more material transported as suspended sediment and, for flocs, allows aggregation and disaggregation processes to continue.

2.2.2. Changes in floc size distribution within the bed

Changes in the size-class distribution of flocs are expected once they have been incorporated into the seabed, in contrast to non-cohesive particles that retain their properties during cycles of erosion and deposition. For example, it seems unlikely that large, low-density flocs can be buried and later resuspended intact, and limited published observations suggest that material

deposited as flocs can be eroded as denser, more angular aggregates (Stone et al., 2008). However, we find little guidance for constraining this process. We therefore have implemented deflocculation, a simple process that stipulates an equilibrium cohesive size-class distribution and an associated relaxation time scale. The time-varying size-class distribution in the bed tends toward the user-specified equilibrium distribution while conserving mass (see Supplement). This influences the amount of material in classes that are available for resuspension when a cohesive bed is eroded. Example cases presented below demonstrate the effect of this process and the associated time scale on floc distributions both in the bed and in the water column.

2.3 Stratigraphy

Stratigraphy serves two functions in the model as conditions change and sediment is added or removed from the bed: (1) to represent the mixture of sediment available at the sediment-water interface for use in bedload transport, sediment resuspension, and roughness calculations; and (2) to record the depositional history of sediment. Bookkeeping methods for tracking and recording stratigraphy must conserve sediment mass and must accurately record and preserve age, porosity, and other bulk properties that apply to each layer. Ideally, a layer could be produced for each time step in which deposition occurs, and a layer could be removed when cumulative erosion exceeds layer thickness. In practice, the design of many models is subject to computational constraints that limit resolution to a finite and relatively small number of layers. In ROMS, this number is declared at the beginning of the model run and cannot change. Thus, when deposition requires a new layer, or when erosion removes a layer, other layers must be split or merged so that the total number of layers remains unchanged. Where and when this is done determines the fidelity and utility of the modeled stratigraphic record. Some models have used a constant layer thickness (Harris and Wiberg, 2001); others (for example, ECOMSED) define layers as isochrons deposited within a fixed time interval (HydroQual, Inc., 2004). Our approach is most similar to that described by Le Hir et al. (2011) in that we allow mixing of deposited material into the top layer, and require a minimum thickness of newly formed layers, merging the bottom layers when a new layer is formed. Likewise, the bottom layer is split when erosion or thickening of the active layer, discussed below, reduces the number of layers. The sequence of layer calculations is described in detail in the Supplement.

A key component of the bed model is the active layer (Hirano, 1971), which is the thin (usually mm-scale), top-most layer of the seabed that participates in exchanges of sediment with the overlying water. During each model time step, deposition and erosion may contribute or remove mass from the active layer. Any stratigraphy in the active layer is lost by instantaneous mixing (Merkel and Klopmann, 2012), but this is consistent with the original concept of Hirano (1971) and the need to represent the spatially averaged surface sediment properties in a grid cell that represents a heterogeneous seabed. The thickness of the active layer in ROMS scales with excess shear stress (Harris and Wiberg, 1997; Warner et al., 2008) and is at least a few median grain diameters thick (Harris and Wiberg, 1997; see Supplement).

Geosci. Model Dev. Discuss., https://doi.org/10.5194/gmd-2017-267
Manuscript under review for journal Geosci. Model Dev.
Discussion started: 1 December 2017

2.4 Bulk Critical Shear Stress for Erosion for Cohesive Sediment

An important difference between cohesive and non-cohesive sediment behavior is that the erodibility of cohesive sediment is treated primarily as a bulk property of the bed, whereas the erodibility of non-cohesive sediment is treated as the property of individual sediment classes. The erodibility of cohesive sediment often decreases with depth in the bed, resulting in depth-limited erosion (Type 1 behavior according to Sanford and Maa, 2001). When the cohesive bed module is used, the erodibility of cohesive beds depends on the bulk critical shear stress for erosion τ_{cb} (Pa), which is a property of the bed layer, not individual sediment classes, and generally increases with depth in the bed. It also changes with time through swelling and consolidation and, in the uppermost layer, is affected by erosion and deposition. The cohesive bed model tracks these changes by updating profiles of τ_{cb} at each grid point during each baroclinic timestep.

There is no generally accepted physically based model for determining τ_{cb} from bed properties such as particle size, mineralogy, and porosity. We adopted Sanford's (2008) heuristic approach based on the concept that the bulk critical shear stress profile tends toward an equilibrium profile that depends on depth in the seabed (Figure 1) and must be determined a priori. Erosion-chamber measurements (Sanford, 2008; Rinehimer et al., 2008; Dickhudt et al., 2009; Dickhudt et al., 2011; Butman et al., 2014) have been used to define equilibrium bulk critical shear stress profiles τ_{cbeq} in terms of an exponential profile defined by a slope and offset.

$$\tau_{cb\,eq} = a \exp\left[\left(\ln\left(z_\rho\right) - offset\right) / slope\right] \tag{3}$$

where z_ρ (kg/m^2) is mass depth, the cumulative dry mass of sediment overlying a given depth in the bed. In Equation 3, *offset* and *slope* have units of ln(kg/m^2), and a = 1 Pa kg^{-1} m^2 is a dummy coefficient that produces the correct units of critical shear stress. The mass depth at the bottom of each model layer k is calculated as

$$z_\rho(k) = \sum_k \sum_i f_{i,k} \rho_i \Delta z_k \tag{4}$$

where the summations are computed over the k bed layers and i sediment classes, f_i (dimensionless) is the fractional amount of sediment class i, ρ_i (kg/m^3) is particle density in class i, and Δz_k (m) is the thickness of layer k. Equation 3 can be written in terms of the power-law fits to erosion-chamber measurements presented by Dickhudt (2008) and Rinehimer et al. (2008; see Supplement). The instantaneous bulk critical shear stress profile is nudged over time scale T_c or T_s (s) toward the equilibrium profile to represent the effects of consolidation or swelling following perturbations caused by erosion or deposition. T_c is the time scale for consolidation and is applied when the instantaneous profile is more erodible than the

equilibrium value, while T_s is the time scale for swelling and is applied when the instantaneous profile is less erodible than the equilibrium value. The consolidation time scale is usually chosen to be much shorter than the one associated with swelling (Sanford, 2008). New sediment deposited to the surface layer is assigned a bulk critical shear stress that may either be (1) held constant at a low value (Rinehimer et al. 2008), or (2) set at the instantaneous bed shear stress of the flow.

2.5 Mixed Sediment

Mixed-sediment processes occur when both cohesive and non-cohesive sediment are present, and are typically sensitive to the proportion of mud. Beds with very low mud content (<3%; Mitchener and Torfs, 1996) behave as non-cohesive sediment: erodibility is determined by particle critical shear stress, which is an intrinsic characteristic of each particle class. Non-cohesive beds may be winnowed and armored by selective erosion of the finer fraction. In contrast, beds with more than 3% to 15-30% (Mitchener and Torfs, 1996; Panagiotopoulos et al., 1997, van Ledden et al., 2004; Jacobs et al, 2011) mud content behave according to bulk properties that, in reality, depend on porosity, mineralogy, organic content, age, burial depth, etc., but that, in the model, are characterized by the bulk critical shear stress for erosion. Mixed beds in the model have low to moderate mud content (3% to 30%, subject to user specification) and their critical shear stress in the model is a weighted combination of cohesive and non-cohesive values determined by the cohesive-behavior parameter P_c, which ranges from 0 (non-cohesive) to 1 (cohesive; see Supplement). This approach allows fine material (e.g., clay) to be easily resuspended when P_c is low and only a small fraction of mud is present in an otherwise sandy bed, and it limits the flux to the amount available in the active mixed layer. It also allows non-cohesive silt or fine sand embedded in an otherwise muddy bed to be resuspended during bulk erosion events when P_c is high, and it provides a simple and smooth transition between these behaviors. The thickness of the active mixed layer is calculated as the thicker of the cohesive and non-cohesive estimates. Figure 2 illustrates mixed-bed behavior as the mud (in this case, clay-sized) fraction f_c increases for a constant bottom stress of 0.12 Pa. At low f_c, P_c is zero (Figure 2a), and clay and silt are easily eroded (high relative flux rates out of the bed; Figure 2c) because the particle critical shear stress for non-cohesive behavior of these fine particles is low (Figure 2b). The relative flux rates in Figure 2b are normalized by the fractional amount of each class and the erosion-rate coefficient; the actual erosional fluxes for clay content would be low at $P_c = 0$ because of the low clay content in the bed. As f_c increases and the bed becomes more cohesive, relative erosion flux rates decline. When f_c exceeds a critical value (0.2 in the example shown in Figure 2), the bed is completely cohesive and erosion fluxes are determined by bulk critical shear stress for erosion of cohesive sediment τ_{cb}.

Geosci. Model Dev. Discuss., https://doi.org/10.5194/gmd-2017-267
Manuscript under review for journal Geosci. Model Dev.
Discussion started: 1 December 2017

2.6 Bed Mixing and Stratigraphy

Mixing of bed properties in sediment can be caused by benthic fauna (ingestion, defecation, or motion such as burrowing) or circulation of porewater, and tends to smooth gradients in stratigraphy and move material vertically in sediment. The model (e.g., Boudreau, 1997) assumes that mixing is a one-dimensional vertical diffusive process and neglects non-local and lateral mixing processes:

$$\frac{\partial C_v}{\partial t} = \frac{\partial}{\partial z}\left(D_b \frac{\partial C_v}{\partial z} \right) \tag{5}$$

where C_v is the volume concentration of a conservative property (e.g., fractional concentration of sediment classes or porosity), D_b is a (bio)diffusion coefficient (m^2/s) that may vary with depth in the bed (see below), and z (m) is depth in the bed (zero at the sediment-water interface, positive downward). We have discretized equation (5) using the varying bed thicknesses and solve it at each baroclinic time step using an implicit method that is stable and accurate (See Supplement).

Biodiffusivity is generally expected to decrease with depth in the sediment (Swift et al., 1994; 1996), but is often assumed to be uniform near the sediment-water interface. The typical depth of uniform mixing, based on worldwide estimates using radionuclide profiles from cores, is 9.8±4.5 cm (Boudreau, 1994). Rates of biodiffusion estimated from profiles of excess ^{234}Th on a muddy mid-shelf deposit off Palos Verdes (California, USA) varied from ~2 cm^2/yr to ~80 cm^2/yr (Wheatcroft and Martin, 1996; Sherwood et al., 2002) and values from the literature range from 0.01 – 100 cm^2/yr (Boudreau, 1997; Lecroart et al., 2010). The depth-dependent biodiffusion rate profile in the model must be specified for each horizontal grid cell using a generalized shape described in the Supplement.

Representation of seabed properties, i.e. the stratigraphy, has been modified slightly from the framework presented in Warner et al. (2008). The revised bed model gives the user latitude to control the resolution of the bed model through the choice of new layer thickness and the number of bed layers, and avoids the mixing described by Merkel and Klopmann (2012). The bookkeeping for bed layers is detailed in the Supplement. The main differences from previous versions of the model (Warner et al., 2008) are the treatments of the second layer (immediately below the active layer) and the bottom layer. During deposition, the new algorithm prevents the second layer from becoming thicker than a user-specifed value, which results in thinner layers that can record changes in sediment composition inherited from the active layer as materials settle. During erosion, the new algorithm splits off only a small portion of the bottom layer to create a new layer. This limits the influence of the initial stratigraphy specified for the bottom layer and confines blurring of the stratigraphic record to the

bottommost layers. Our tests indicate the new approach provides a more informative record of stratigraphic changes. Moriarty et al. (2017) used a similar approach to bed stratigraphy to preserve spatial gradients in sediment biogeochemistry.

3 Demonstration Cases

The following cases demonstrate the cohesive-sediment processes included in ROMS, explore model sensitivity to parameters, and provide candidates for inter-model comparisons.

3.1 Floc Model

Tests using a quasi one-dimensional vertical implementation of ROMS were conducted to verify that the floc model was implemented correctly and to gain some insight into model behavior under typical coastal conditions.

3.1.1 Comparison with laboratory experiments

Verney et al. (2011) compared results from FLOCMOD with a laboratory experiment of tidal-cycle variation in shear rate G. We performed the same simulations in ROMS by initializing with the same floc model parameters and specified $G(t)$, ranging from G=0 s^{-1} at slack tide to G=12 s^{-1} at peak flow. The model was run with 15 cohesive classes (instead of the 100 classes in the reference FLOCMOD experiment). The class sizes were log-spaced between 4 and 1500 µm with floc densities derived from Equation 1 using n_f = 1.9. The initial suspended-sediment concentration was 0.093 kg/m^3 in the 120-µm class. Our results (Figure 3a) matched the cycles of floc diameter variation caused by aggregation (low G) and breakup (high G) shown in Figure 7 of Verney et al. (2011), with a 24-µm root-mean square (rms) difference from observations in mass-weighted mean diameter.

We also compared our ROMS FLOCMOD implementation with laboratory experiments of the growth and breakup of flocs performed by Keyvani and Strom (2014) who applied cycles of G=15 s^{-1} that caused floc growth followed by long periods (15 h) of very strong turbulent shear rates (G=400 s^{-1}) that caused disaggregation. We simulated the first cycle of floc formation using the size classes, fractal dimension, and concentrations provided by Keyvani and Strom (2014), but varying the aggregation parameter α and the breakup parameter β that determine the final equilibrium diameter. Our model results with α=0.1 and β=0.0135 (Figure 3b) reproduced the observations with higher skill than the simple model used in their study. The same final diameter was obtained with α=0.45 and β=0.06, but the equilibrium was attained more quickly than observed.

These comparisons with laboratory results indicated that our implementation of FLOCMOD in ROMS was correct and demonstrated that the model has useful skill in representing floc dynamics

Geosci. Model Dev. Discuss., https://doi.org/10.5194/gmd-2017-267
Manuscript under review for journal Geosci. Model Dev.
Discussion started: 1 December 2017

3.1.2. Comparison to equilibrium floc size

Simulations were conducted to further evaluate the ROMS implementation of FLOCMOD by comparing modeled equilibrium floc sizes to equilibrium floc sizes predicted by Winterwerp (2006). He argued that, in steady conditions, equilibrium floc sizes are determined by the fractal dimension n_f, ratio of aggregation rates and breakup rates, concentration C (kg/m^3), and turbulence shear rate G (s^{-1}). The equilibrium median floc size D_{50} (m) is given by

$$D_{50} = D_p + \frac{k_A}{k_B}\frac{C}{\sqrt{G}} \tag{6}$$

where k_A and k_B are aggregation and breakup coefficients, respectively (Winterwerp, 1998). The units of k_A and k_B depend on fractal dimensions, but the ratio has units of m^{4}kg^{-1}s$^{-1/2}$. We compared our FLOCMOD results with this theoretical relationship by running cases with steady conditions, n_f = 2, for a range of concentrations (C = 0.1 to 10 kg/m^3), a range of shear rates (G = 0.025 to 100 s^{-1}), and several combinations of aggregation and breakup parameters α and β. The results show that equilibrium floc size increases with concentration and decreases with turbulence shear rate, as expected (Figure 3c). Equilibrium diameter is strongly controlled by concentration, and turbulence is more effective at reducing average diameter at lower concentrations. The slope of the relationship between the equilibrium diameter and $C/\sqrt{G}$ varies with the ratio of aggregation to breakup. Winterwerp (1998) suggested a slope of about 4x10^3 m^{4}kg^{-1}s$^{-1/2}$. Figure 3c demonstrates that a range of slopes can be obtained by varying the ratio α/β. The model reproduced the linear response predicted by Winterwerp (1998) except near the largest sizes, where our upper limit in floc class size (5000 µm) distorted the statistics. Although not shown in Figure 3c, the floc populations evolved at different rates, depending on α and β, as indicated in Figure 3b.

3.1.3. Evolution to steady state

Steady, uniform flow is a conceptually simple model test that demonstrates the hydrodynamics linking vertical profiles of flow, evolution of the turbulent boundary layer, and bottom drag. The addition of floc dynamics creates a complicated and instructive test case. This simulation, forced by a constant sea-surface slope, is similar to the steady flow test examined by Winterwerp (2002, section 4.8.1), and produces a linear Reynolds-stress profile increasing from zero at the surface to $\tau_b = -\rho_w g h\, ds/dx$ at the seabed, where τ_b (Pa) is bottom shear stress, g (m/s^2) is gravitational acceleration, h (m) is water depth, and ds/dx (m/m) is sea-surface slope. The flow develops a logarithmic velocity profile $u = (u_* / \kappa)\ln(z/z_o)$, where u (m/s) is velocity in the x direction, $u_* = \sqrt{\tau_b/\rho_w}$ is shear velocity (m/s), $\kappa = 0.41$ (dimensionless) is von Kármán's

362 constant, z (m) is elevation above the bed, and z_0 (m) is the bottom roughness length. The final flow velocity near the
363 surface is about 0.6 m/s. When non-cohesive sediment is added (and erosion and deposition are set to zero), the suspended
364 sediment concentrations for each size class evolve into Rouse-like profiles where, at each elevation, downward settling is
365 balanced by upward diffusion. The addition of floc dynamics complicates the situation, because aggregation creates larger
366 flocs with higher settling velocities. The larger flocs tend to settle into regions of higher shear and higher concentration,
367 where the higher shear tends to break them into smaller flocs but the higher concentrations enhance aggregation. The size
368 distribution, settling velocity, concentration, shear, and turbulent diffusion evolve to a steady state under a dynamic balance.
369 The resulting profiles of concentration and mass-weighted average size and settling velocity are sensitive to both floc model
370 parameters and modeled physical conditions (water depth, bottom stress, turbulence model, total sediment in suspension).

371 We demonstrate this process using 22 floc classes with logarithmically spaced diameters ranging from 4 to 5000 μm (Figure
372 4). The initial vertical concentration profile was uniform at 0.2 kg/m^3, all in the 8-μm class. The model started from rest, and
373 the initial response was slow particle settling in the nearly inviscid flow: concentrations, floc sizes, and settling velocities all
374 decreased near the surface (Figures 4a, b, and c). As the flow accelerated in the first two hours, turbulence generated by
375 shear at the bottom began to mix upward in the water column, diffusing settled material higher and facilitating collisions and
376 aggregation among flocs. Between hours 3 and 4, settling was enhanced by these newly formed larger flocs, as is apparent in
377 increases in average diameter and settling velocities, and reduced concentrations near the surface. Equilibrium was nearly
378 established by about hour 5. At the end of the model run, the total concentration profile decreased exponentially with
379 elevation (Figure 4d and 4g), but average size and settling velocities both decreased markedly in the bottom meter (Figures
380 4e and 4f), reflecting shear disaggregation that lead to increases in smaller flocs near the bottom (Figure 4g).

381 The time scales to achieve equilibrium in this simulation are comparable to tidal time scales, suggesting equilibrium is
382 unlikely in the real world, where forcing is time dependent and bottom conditions are spatially variable. The final condition
383 is sensitive to flow forcing, initial concentrations, and floc parameters. For example, when concentrations are higher, or
384 when the disaggregation parameter is increased (making the flocs more fragile), bottom-generated shear causes
385 disaggregation higher into the water column, and mid-depth maxima in diameter and settling velocity evolve. This steady
386 flow simulation is useful as both a standard test case and a reminder of the complexity of floc processes, even when the
387 hydrodynamics are relatively simple.

388 **3.1.4. Settling fluxes**

389 Interaction with the bed influences the evolution of the floc population in the water column by providing sources or sinks in
390 various size classes. We have experimented with several sediment-flux conditions from the water column to the seabed,

including settling fluxes, zero fluxes, and fluxes modulated by threshold stresses for deposition. Settling fluxes calculated as $w_k \rho_k C_k \Delta t$ summed over each class *k*, is the default method used for non-cohesive sediment. Zero-flux boundary conditions essentially treat the bottom water-column cell as a fluff layer, allowing flocs to accumulate by settling or mix out by diffusion. Floc dynamics continue to operate in this layer, so the size distributions change with concentration and stress. Settling fluxes modulated by stress thresholds for deposition allow flocs to deposit only under relatively quiescent conditions. The model framework provides a variety of choices described in the Supplement, each with implications that must be assessed in the context of the problem at hand. As expected, the conditions that reduced settling into the bed resulted in higher sediment concentrations in the bottommost water-column layer and allowed for floc breakup by the enhanced near-bottom turbulence.

3.1.5. Model sensitivity

A wide range of model runs (not presented here) have provided us with a qualitative sense of model performance. Model results respond as expected to physical parameters, such as mean concentration and shear rate (discussed above), as well as primary particle size and fractal dimension. Model results are also sensitive to model configuration, including the number of size classes, the size of vertical grid spacing, and the time step used. Our experience so far confirms that of Verney et al. (2011): a truncated distribution of about seven size classes provides qualitatively useful results, but the choice of size range and size distribution may change the results. The sensitivity to vertical grid resolution is particularly important in the bottommost layer, which has the highest concentrations and highest shear rates. Finer grid spacing near the bottom results in layers with higher shear and higher sediment concentrations, which cause local changes in the equilibrium floc sizes. Model time steps in our floc model tests are short, ranging from 10 to (more typically) 1 s. The adaptive sub-steps for aggregation and disaggregation were limited to a minimum of 0.5 s. At high concentrations (> 0.2 kg/m^3) and high shear rates, the results sometimes showed numerical instability, probably related to the explicit solution of Equations 2. Replacement of the solver for these equations with a faster and more robust method in the future should improve model stability.

3.2 Resuspension

Three cases are presented here to demonstrate the evolution of stratigraphy caused by resuspension and subsequent settling of sediment during time-dependent bottom shear stress events. They contrast model calculations using the non-cohesive and mixed-bed routines, and highlight the role of biodiffusion. These were one-dimensional (vertical) cases represented with small (~5 x 6 horizontal x 20 vertical cells), three-dimensional domains with flat bottoms and periodic lateral boundary conditions on all sides. They were forced with time-varying surface wind stress that generated time-dependent horizontal velocities and bottom stress, initialized with zero velocity and zero suspended-sediment concentration, and did not include floc dynamics in the water column.

Geosci. Model Dev. Discuss., https://doi.org/10.5194/gmd-2017-267
Manuscript under review for journal Geosci. Model Dev.
Discussion started: 1 December 2017

3.2.1 Non-cohesive bed simulation

A non-cohesive bed simulation was used to demonstrate the generation and preservation of sand and silt stratigraphy during a resuspension and settling event (Figure 5). The model was forced with two stress events ~ 1.5 d apart and lasting 1.5 d and 1 d respectively. Four sediment classes, representing particles with nominal diameters of 4, 30, 62.5, and 140 μm, particle critical shear stresses of 0.05, 0.05, 0.1, and 0.1 Pa, and settling velocities of 0.1, 0.6, 2, and 8 mm s^{-1} were used. Although the diameters of the first two sediment classes corresponded to mud, all sediment classes in this experiment were treated as non-cohesive material. The initial sediment bed contained 41 layers, each 1 mm thick, and each holding equal fractions (25%) of the four sediment classes. New sediment layers were constrained to be no more than 1 mm thick.

The first, larger stress event (maximum τ_b = 1 Pa; Figure 5b), eroded 1.2 cm of bed, and recruited additional fine sediment from the active layer, which extended 2 cm below the initial sediment surface (Figure 5d). The finer fractions dominated the suspended sediment in the water column, which contained only a small fraction of the coarsest sand (Figure 5a). When the stress subsided, coarser sediment deposited first, while finer material remained suspended, producing graded bedding above the 2-cm limit of initial disturbance (Figure 5d). The second stress pulse eroded the bed down to 1 cm but only resuspended minimal amounts of the 140- μm sand. Deposition resumed after the second pulse subsided and, at the end of the simulation, some mud remained in the water column (Figure 5a), leaving the bed with net erosion of 5 mm (Figure 5d). The finest material (4 μm) remained mostly in suspension after five days. The final thickness of the bottom five layers was smaller than their initial value (1 mm), because, to maintain a constant number of bed layers, the deepest layer was split each time a surface layer was formed during deposition. The two stress pulses affected sediment texture down to 2 cm. Above this level, almost all of the finest class was winnowed, and remained mostly in suspension while the other classes settled to the bed, so that the upper bed layers developed a fining-upward storm layer. The bottom portion of the storm layer (1 – 2 cm depth) was a lag layer comprised of the two coarsest classes, both because these resisted erosion and because the sand that did erode settled to the bed quickly when shear stress decreased.

3.2.2 Mixed bed simulation

This case examined the stratigraphic consequences of cohesive behavior resulting from a single bottom-stress event (Figure 6). The model configuration was similar to the previous example. The same sediment classes were used, but the two finest (4 and 30 μm) were treated as cohesive mud, while the other two remained non-cohesive (sand). The fraction of cohesive sediment (f_c = 0.5) exceeded the chosen non-cohesive threshold (f_{nc} threshold = 0.2), so the bed behaved as if it were completely cohesive. The cohesive formulation required the initialization of an equilibrium bulk critical stress profile for erosion $\tau_{cb\,eq}(z)$. We chose parameters within the range of sensitivities studied by Rinehimer et al. (2008) and specified an

equilibrium profile with a *slope* = 2 ln(kg/m^2) and an *offset* of 3.4 ln(kg/m^2), with a minimum value of 0.03 Pa and a maximum of 1.5 Pa (dashed magenta line in Figure 6b) and initialized the model with this profile (solid purple line in Figure 6b). The time scale for consolidation was set to T_c= 8 hours. The swelling time scale was chosen to be 100 times longer than consolidation (T_s = 33 days). A time series of bed stress was imposed (Figure 6a), and the bed responded initially by eroding. As the imposed stress waned starting at day 1.8, sediment settled to the bed causing deposition. The initial rapid increase in bottom stress during the first 0.7 days (Figure 6a) exceeded the critical stress of the bed to a depth of 2.4 cm (red line in Figure 6c), causing resuspension and erosion of the top 5 mm of the bed. In this case, the amount of material eroded was limited by the erosion rate coefficient. The equilibrium critical stress profile, which has a static shape, shifted down with the sediment-water interface (compare dashed magenta line in Figures 6b, c). After the initial erosion, the instantaneous critical stress profile tended toward the equilibrium critical stress profile over the slow swelling time scale of 33 days, rendering the bed a little more erodible (compare Figures 6c, d). By day 2.8, the stress had waned and 4 mm of sediment had redeposited (Figure 6d). The equilibrium critical stress profile had shifted upward with the bed surface, causing the instantaneous critical stress to increase over the short compaction time scale. The final instantaneous critical shear stress profile (Figure 6e) had reached the long-term equilibrium everywhere except in the most recent deposits. This case exemplifies the sequence of depth-limited erosion, deposition, and compaction that characterizes the response of mixed and cohesive sediment in the model.

3.2.3 Biodiffusion simulations

We validated the numerical performance of the biodiffusion algorithms using two analytical test cases with a realistic range of parameters. The implicit numerical solution is unconditionally stable and conserves mass to within 10^{-8} %, but the accuracy depends on time step, gradients in biodiffusivity, and bed thickness. Typical RMS differences in the fractional amount of sediment in a particular class between the numerical solutions and the analytical solutions ranged from 10^{-2} to 10^{-6}. We found that, for modeled beds 5 m thick, solutions improved as layer thickness decreased from 50 to 5 cm, but beyond that, higher resolution did not substantially improve the solution. Even in the worst case, where the numerical solution was off by 1%, it was much more precise than our estimates of biodiffusivity coefficients.

Four cases are presented to demonstrate bed mixing (Figure 7). The first two used the same configuration as in the non-cohesive (Figures 5, 7a) and mixed-bed simulations (Figures 6d, 7b). The second two were identical to the mixed-bed case except that biodiffusive mixing was enabled. The biodiffusivity profile used was similar to that proposed for the mid-shelf deposit offshore of Palos Verdes, CA (Sherwood et al., 2002) that had a constant diffusivity D_{bs} from the sediment-water interface down to 2 mm, an exponential decrease between 2 mm and 8 mm, and a linear decrease to zero at 1 cm depth.

These two cases differed in their biodiffusion coefficients: a) the first used relatively large biodiffusion coefficients (D_{bs} = 10^{-5} m^2s^{-1}); b) the second used smaller values (D_{bs} = 10^{-10} m^2s^{-1}).

The resulting stratigraphy after the five-day simulation (Figure 7) indicates that mixing in the case with large biodiffusivity (Figure 7c) tended to smooth all gradients rapidly and only during depositional conditions was the vertical structure of grain size fractions preserved. Some sediment remained in suspension in all four cases, which was reflected in the final bed elevation. The resulting top 1 cm of the bed was always well mixed and the depth of the disturbed sediment at the end of the simulation was deeper (2.5 cm) in this case than in the other simulations. Sediment deeper than 2.5 cm below the surface was undisturbed: it was beyond the reach of erosion, active-layer formation, and biodiffusion. The biodiffusive mixing increased recruitment of fine sediment into the surface active layer during erosion, resulting in increased concentrations in the water column (not shown) compared to the mixed bed case without biodiffusion.

The case with a smaller biodiffusion coefficient (Figure 7d) developed stratigraphy intermediate to those cases with large and zero biodiffusion. The depth of disturbed sediment was 2.3 cm and the transition between redeposited sand and mud was smooth with coarse sand being present at the surface of the bed. This gradual size gradation was intermediate to the sharp jump in the fractional distribution between mostly sandy layers and predominantly muddy layers produced in cases that neglected mixing (Figure 7a,b) and the smooth gradient produced by the strong mixing case (Figure 7c).

3.3 Estuarine Turbidity Maxima

High concentrations of suspended sediment often occur near the salt front in estuaries, forming estuary turbidity maxima (ETM). We present ETM test cases that simulated sediment transport in a two-dimensional (longitudinal and vertical) salt-wedge estuary with tidal and riverine forcing. The cases investigated the formation of cohesive deposits beneath the ETM with and without floc dynamics. The first case, without floc dynamics but with a mixed bed, is presented here. The second case, presented below, adds floc dynamics. The model was forced with a 12-hour tidal oscillation modulated with a 14-day spring-neap cycle. The idealized estuary was 100-km long with a sloping bottom 4 m deep at the head of the estuary and 10 m deep at the mouth (Figure 8a). In all cases, the simulations were run for twenty tidal cycles. Two non-cohesive sediment classes (180- and 250-μm diameter) were represented with equal initial bed fractions (50% of each). One cohesive fraction (37 μm, ρ_f = 1200 kg/m^3, w_s = 0.13 mm/s) was included, with an initial uniform suspended-sediment concentration of 1 kg/m^3. The bed was initialized without any cohesive sediment, so it initially behaved non-cohesively. Later in the simulation, bed behavior became mixed as suspended mud settled and was incorporated into the initially sandy bed. The chosen equilibrium bulk critical shear stress profile (Equation 3) had *slope* = 5 ln(kg/m2) and *offset* = 2 ln(kg/m^2), with a minimum value of 0.05 Pa and a maximum of 2.2 Pa. The time scale for consolidation was set to T_c=8 hours (Sanford, 2008; Rinehimer, 2008), and the swelling time scale was set to T_s=33 days.

During the simulations, salinity and suspended-sediment field evolved into dynamic equilibria that were repeated over consecutive tides. An estuarine turbidity maximum (ETM) developed between 10 km and 60 km from the mouth of the estuary (Figure 8a) in the salt wedge generated by gravitational circulation and tidal straining (Burchard and Baumert, 1998; MacCready and Geyer, 2001). Elevated suspended-sediment concentrations ranging from 0.7 to 2.05 kg/m^3 occupied most of the bottom layer and extended to mid-depth. All of the suspended material was in the 37-μm class (Figure 8a).

The second case was identical, except that it included floc dynamics. Fifteen cohesive (floc) classes and the two non-cohesive (sand) classes were included. Floc-class diameters were logarithmically spaced, ranging from 20 to 1500 μm, with floc densities ranging from 1350 to 1029.3 kg/m^3, and settling velocities ranging from 0.078 to 5.31 mm/s, commensurate with Equation 1 with fractal dimension n_f = 2. The suspended-sediment concentration field was initialized with a uniform concentration of 1 kg/m^3, all in the 37-µm class. The resulting ETM (Figure 8b) extended farther up-estuary and contained much lower concentrations (0.1 to 0.5 kg/m^3 in most of the salt wedge, with a thin layer of higher concentrations (2.1 kg/m^3) in the bottom layer (bottom 5% of the water column). The second layer (5 – 10% of the water column) had concentrations about half of the bottom layer. The bed sediment response for the two cases also differed. In the no-floc case, the ETM deposit was slightly thinner, located closer to the mouth, and varied less from slack to flood (Figure 8c). Floc dynamics created large tidal variations in the size of bed material (Figure 8d), which ranged up to 600 μm as flocs deposited during slack, and decreased to 37 μm as flocs were resuspended during flood. The behavior in the unflocculated case was less intuitive. Over the course of the simulation, enough fine material accumulated beneath the ETM to cause the bed to behave cohesively, but the top, active layer remained mostly non-cohesive. During flood tide, bottom stresses were sufficient to resuspend the non-cohesive 70 μm material, leaving the cohesive 37 μm material on the bed. Thus, in both cases, the bed became finer during period of higher stress, but for different reasons. The two cases highlight the model-dependent changes in location (driven primarily by settling velocities) and size distributions (driven by floc dynamics) of the ETM.

We next expanded the numerical experiment, using **s**ix floc cases to elucidate the effects of floc dynamics in the idealized estuary (Table 1). The two-dimensional model domain was the same as the ETM case described above. Three types of floc behavior in the seabed were investigated: (1) no changes in size distribution occurred in the bed; (2) the bed deflocculation process was invoked, which nudged all cohesive sediment into the 20-μm class over a long time scale (50 hours); and (3) the bed deflocculation process was invoked with a short time scale (5 hours). Additionally, three other combinations of aggregation (α) and disaggregation (β) rates were used with the slow deflocculation rate to explore floc processes in the water column (Table 1). The following six metrics were compared at the location of the maximum depth-mean suspended-sediment concentration (SSC): depth-mean SSC; maximum SSC; median size (D_{50}); 12-h mean of the D_{50}; depth-mean settling velocity w_s; and depth-mean w_s averaged over a 12-h tidal period (Table 1). The median size and mean settling

539 velocities were weighted by the mass in each class. Also listed in Table 1 are the locus of the maximum deposition, the
540 thickness at that location, and the median size of deposited material at that location.

541 Mean SSC in the ETM did not vary significantly among the floc cases, but the maximum SSC (located lower in the water
542 column) increased when the ratio of aggregation rate / disaggregation rate α / β was higher, which led to larger, faster-
543 settling flocs. Among the four cases (3 – 6) with slow deflocculation rates in the bed, settling velocities, maximum SSC, and
544 floc size covaried. The locus of maximum deposition of ETM material was insensitive to the deflocculation algorithms
545 (cases 1 – 3), and most sensitive to the overall floc rates. The range of ETM locations is listed in Table 6 to highlight the
546 cases where ETM location varied. The case with lowest floc rates (case 5) produced the farthest upriver deposit, with the
547 most variation in the location of the maximum. The case with the highest settling velocities (case 6) produced deposits
548 closest to the estuary mouth. Overall, the simulated ETM was more sensitive to changes in floc parameters than to prescribed
549 behavior of the floc population in the seabed (deflocculation), and the greatest effect of varying floc dynamics was the
550 vertical location of the ETM, which was controlled by floc size and settling velocity.

551 **4 Realistic Application: York River Estuary**

552 This section demonstrates the cohesive sediment bed model in a realistic domain representing the York River, a sub estuary
553 of Chesapeake Bay (Figure 9). Recent modeling efforts have focused on this location as part of a program aimed at exploring
554 links between cohesive sediment behavior, benthic ecology, and light attenuation. As part of this program, colleagues have
555 obtained complementary field observations there, which have been especially focused on the two locations off Gloucester
556 Point and Clay Bank, VA (e.g. Dickhudt et al. 2009, 2011; Cartwright et al. 2013). The implementation presented here is
557 similar to the three-dimensional model developed by Fall et al. (2014) that accounted for circulation, sediment transport, and
558 a cohesive bed. While this model neglects flocculation, information obtained by field observations such as Cartwright et al.
559 (2013) have been consulted for guidance in setting settling velocities of the cohesive particles. The model is run assuming
560 muddy behavior of the bed, and neglecting mixed bed processes, because the majority of sediment transport within the York
561 River channels consists of fine-grained material. We found that it was important to modify the sediment bed layering
562 management scheme, as discussed in section 5 below, to resolve the high gradients in bed erodibility evident in the sediment
563 bed model (i.e. Fall et all 2014) and data (i.e. Dickhudt et al. 2009, 2011).

564 In this implementation, sediment deposited to the bed provided an easily erodible layer with an assumed low critical stress, τ_c
565 = 0.05 Pa. The modeled sediment bed erodibility and suspended-sediment concentrations both were found to be sensitive to
566 parameterization of the equilibrium critical stress profile, and to the consolidation and swelling timescales used (Fall et al.,

2014). Here we present a case similar to that shown by Fall et al. (2014), but that differs mainly in terms of the sediment bed initialization. The equilibrium critical stress profile was chosen as $\tau_{cb\,eq} = z_p^{0.62}$ which was a power-law fit of erodibility experiments performed by Dickhudt (2008) on field-collected cores in September 2007 (Rinehimer et al., 2008). Swelling and consolidation timescales of 1 day and 50 days, respectively, were used. Both the porosity (ϕ = 0.9) and the erosion rate parameter E_0 = 0.03 kg/(m^2 s Pa) were held constant. A zero-gradient condition was applied for suspended-sediment concentration at the open boundary where the York River meets Chesapeake Bay. Six sediment classes that had settling velocities ranging from 0.032 to 10 mm/s were used. To initialize the seabed, they were distributed in equal fractions throughout the model domain in a 20-layer sediment bed that had a total thickness of 1 m, with all but the bottom layer being thin (0.1 mm). In this way, the model was initialized with a sediment bed that had high vertical resolution (0.1 mm) in the upper ~2 cm, underlain by a thick layer (~1 m) sediment. This created high vertical resolution in the bulk critical shear stress profile near the sediment – water interface, while still providing a fairly large pool of sediment so that erosional locations retained some sediment in the seabed throughout the model run. Bed critical stress was initialized everywhere to be constant (0.05 Pa) with depth, and quickly evolved to the equilibrium critical shear stress profile at the compaction time scale of a few days. The model was run to represent two months using the sixty-year median freshwater flow of 67 m^3/s and a spring-neap tidal cycle with 0.2-m neap amplitude and 0.4-m spring amplitude.

The initially uniform bed evolved during the 60-day model run, developing areas of high sediment erodibility along the shoals of the estuary and channel flanks (Figure 10a). In general, sediment was removed from the main channel, which developed reduced erodibility (Figure 10a). At the Gloucester Point site, the initial bed evolved to become less erodible, with a critical shear stress at the seabed that exceeded the equilibrium values specified for the model (Figure 10a). Conversely, at the Clay Bank field site, conditions were variable in space. Sediment deposited on the shoal area, which evolved to enhanced erodibility (Figure 10a). Within the channel, however, the equilibrium critical stress for erosion was often exceeded, resulting in a strongly eroded sediment bed having larger values of critical shear at the sediment surface (Figure 10a). Resuspension and transport also changed the spatial distribution of sediment classes, with the erosional areas retaining only the coarser, faster-settling classes, while depositional areas retained finer-grained, slower-settling particles (Figure 10 b, c). These patterns, with coarse lag layers and reduced erodibility in the channels relative to the shoals, are consistent with the known grain size distributions and properties of the York River Estuary.

5 Discussion

The model algorithms presented here were motivated by the need to improve the representations of sediment dynamics in numerical models of fine-grained and mixed-sediment environments. The improvements were implemented in the COAWST

version of ROMS, which provides a framework for realistic two-way nested models with forcing from meteorology and waves. ROMS includes options for several turbulence sub-models (e.g., $k-\varepsilon$, $k-\omega$, Mellor-Yamada) and wave-current bottom-boundary layer sub-models that allow us to calculate fields of shear velocity G. Implementation of FLOCMOD in this framework provides a platform for numerical experiments and real-world applications of a full-featured floc model.

The primary role of the floc model is to simulate the dynamical response of particle settling velocities to spatial and temporal variations in shear and suspended-sediment concentrations. This can also be achieved with simpler and computationally more efficient parameterization in many applications. What are the advantages of the complex and much slower model implemented here? There are several. The floc model provides fields of particles with dynamically varying density and number of primary particles, which allow calculation of the acoustic and optical responses of the particle fields. In turn, this allows direct comparison with field measurements of light attenuation, optical backscatterance, and acoustic backscatterance, the de facto proxies for suspended-sediment concentration. This also allows calculation of derived properties in the water column, including light penetration and diver visibility. Finally, the modeled particle properties can be used in geochemical calculations that require estimates of particle radius, porosity, and reactive surface area. Depending on the application, this additional information may justify the computational expense of the floc model.

The cohesive bed model provides a heuristic but demonstrably useful tool for representing muddy and mixed beds. The cohesive bed framework captures the most important aspects of muddy environment: limitations on erosion caused by increased bed strength with depth in the sediment, and changes toward user-defined equilibrium conditions as deposited (or eroded) beds age. The physical processes of self-compaction and associated changes in porosity and bed strength are not modeled, but the framework of particle-class and bed-layer variables are designed to accommodate a compaction algorithm. The equilibrium profile method implemented here adds little computational expense, but allows the model to represent depth-limited erosion, a key property of many cohesive beds.

Modeling stratigraphy effectively is challenging. Although conserving sediment mass among a fixed number of layers is straightforward, it has proven difficult to devise a robust and efficient method that records relevant stratigraphic events in a modeled sediment bed over the wide range of conditions that occur in coastal domains. For both sediment transport and sediment bed geochemistry (i.e. Moriarty et al. 2017), it can be important for the sediment bed model to achieve its highest vertical resolution near the sediment – water interface, but the original ROMS sediment bed model did not meet that goal when the sediment bed was subject to frequent or repeated cycles of erosion. The modifications we have made to the bed-layer management have improved the fidelity with which we can record stratigraphic events in the model layers, particularly at the sediment – water interface. Inclusion of biodiffusive mixing is important for environments where biological activity is rapid, compared with sedimentation or physical reworking. Additionally, for problems of sediment geochemistry, it is important to account for mixing of both particulate matter and porewater. Expansion of the ROMS sediment bed model to

include diffusive mixing facilitates its use for interdisciplinary problems (i.e. Moriarty et al. 2017). The choice of appropriate mixing parameters remains a challenge, especially when considering the spatial and seasonal heterogeneity of biological activity.

Overall, the cohesive and mixed-bed algorithms we have introduced in ROMS provide tools that should be useful for both numerical experimentations and realistic applications for fine-grained, and mixed-bed environments. Our implementation of flocculation, bed consolidation, and bed-mixing modules enhance the utility of the ROMS sediment model for interdisciplinary studies including ecosystem feedbacks (light attenuation, biogeochemistry), and contaminant transport.

6 Conclusion

This paper describes three ways in which the sediment model of Warner et al. (2008) has been enhanced, allowing simulations to be made for non-cohesive, cohesive, and mixed sediment and allowing it to be applied in a wider range of studies. A flocculation model has been added, following Verney et al. (2011). The cohesive bed model developed by Sanford (2008) has been added, allowing the erodibility of the sediment bed to evolve in response to the erosional and depositional history. Mixing between bed layers has been implemented as biodiffusion using a user-specified diffusion coefficient profile. In addition, the sediment bed layering routine has been modified so that bed layers maintain a high resolution near the sediment water interface, as demonstrated by both our idealized and realistic case studies presented here. The paper presents results of model runs that test and demonstrate these new features and to show their application to real-world systems. The authors encourage the coastal modeling community to use, evaluate, and improve upon the new routines.

Code and Data Availability

The algorithms described here have been implemented in ROMS (version 3.6) distributed with the Coupled Ocean Atmosphere Waves Sediment-Transport Modeling System (COAWST, Subversion repository revision number 1179). COAWST is an open-source community modeling system with a Subversion source-control system maintained by John C. Warner (jcwarner@usgs.gov) and distributed under the MIT/X License (Warner et al., 2010). The COAWST distribution files contain source code derived from ROMS, WRF, SWAN, MCT, and SCRIP, along with Matlab code, examples, and a User's Manual.

651 **Supplement Link (supplied by Copernicus)**

652 **Team List**

653 **Author Contribution**

654 C.R. Sherwood and A. Aretxabaleta shared development of the model code and test cases and most of the manuscript
655 preparation. J.P. Rineheimer was an early user of the cohesive bed model and, along with C.K. Harris, developed the York
656 River application. R. Verney graciously supplied his FORTRAN version of FLOCMOD and helped with adaptation for
657 ROMS. B. Ferré contributed to the early development and application of the model. All authors contributed to the final
658 version.

659 **Competing Interests**

660 The authors declare that they have no conflict of interest.

661 **Disclaimer**

662 Use of firm and product names is for descriptive purposes only and does not imply endorsement by the U.S. Government.

663 **Special Issue Statement - None**

664 **Acknlowledgements**

665 The authors thank Jeremy Spearman, Alexis Beudin, Julia Moriarity and two anonymous reviewers for helpful comments on
666 earlier drafts of this manuscript. This work was been supported by the U.S. Geological Survey, Coastal and Marine Geology
667 Program and the National Ocean Partnership Program. C.K. Harris was supported by NSF (OCE-1459708, OCE-1061781,
668 and OCE-0536572). This is contribution number XXXX of the Virginia Institute of Marine Sciences. B. Ferré is affiliated
669 with the Centre of Excellence: Arctic Gas hydrate, Environment and Climate (CAGE) funded by the Norwegian Research
670 Council (grant no. 223259). The model code is implemented in ROMS version 3.6, as distributed with the COAWST
671 modeling system (Subversion repository revision 1179; Warner et al., 2010), and is freely available by request to John C.
672 Warner (jcwarner@usgs.gov) at the U.S. Geological Survey.

673 **References**

674 Amoudry, L. O., and Souza, A. J.: Deterministic coastal morphological and sediment transport modeling: a review and
675 discussion, Rev. Geophys., 49 (RG2002), 21, doi:10.1029/2010RG000341, 2011.

676 Ariathurai, R., Arulanandan, K., Erosion Rates of Cohesive Soils, ASCE Journal of the Hydraulics Division 104, 279–283,
677 1978.

678 Boudreau B. P.: Is burial velocity a master parameter for bioturbation? Geochim. Cosmochim. Ac., 58, 1243-1250, 1994.

679 Boudreau, B. P.: Diagenetic Models and Their Implementation, Springer-Verlag, Berlin, 414 pp, 1997.

680 Beudin, A., Kalra, T. S., Ganju, N. K., and Warner, J. C.: Development of a Coupled Wave-Flow-Vegetation Interaction
681 Model, Comput. Geosci.100, 76–86, doi:10.1016/j.cageo.2016.12.010, 2017.

682 Burchard, H. and Baumert, H.: The formation of estuary turbidity maxima due to density effects in the salt wedge. A
683 hydrodynamic process study, J. Phys. Oceanogr., 20, 2, 309–321, 1998.

684 Butman B., Aretxabaleta, A. L., Dickhudt, P. J., Dalyander, P. S., Sherwood, C. R., Anderson, D. M., Keafer, B. A., and
685 Signell, R. P.: Investigating the importance of sediment resuspension in Alexandrium fundyense cyst population
686 dynamics in the Gulf of Maine, Deep-Sea Res. PT II, 103, 74–95, doi:10.1016/j.dsr2.2013.10.011, 2014.

687 Caldwell, R. L., and Edmonds, D. A.: The effects of sediment properties on deltaic processes and morphologies: A
688 numerical modeling study, J. Geophys. Res. Earth Surf., 119, 961–982, doi:10.1002/2013JF002965, 2014.

689 Cartwright, G.M., C.T. Friedrichs, C.T., and Smith, J. S.: A test of the ADV-based Reynolds-flux method for in situ
690 estimation of sediment settling velocity in a muddy estuary. Geo-Marine Letters, 33: 477-484.
691 http://dx.doi.org/10.1007/s00367-013-0340-4, 2013.

692 del Barrio, P., Ganju, N. K., Aretxabaleta, A. L., Hayn, M., García, A., and Howarth, R. W.: Modeling Future Scenarios of
693 Light Attenuation and Potential Seagrass Success in a Eutrophic Estuary, Estuar. Coast. Shelf Sci., 149, 13–23,
694 doi:10.1016/j.ecss.2014.07.005, 2014.

695 Dickhudt, P. J.: Controls on erodibility in a partially mixed estuary: York River, Virginia, M. S. Thesis, College of William
696 and Mary, Gloucester Point, VA, 2008.

697 Dickhudt, P. J., Friedrichs, C. T., Schaffner, L. C., and Sanford, L. P.: Spatial and temporal variation in cohesive sediment
698 erodibility in the York River estuary, eastern USA: A biologically influenced equilibrium modified by seasonal
699 deposition, Mar. Geol., 267, 3–4, 128–140. doi:10.1016/j.margeo.2009.09.009, 2009.

700 Dickhudt, P. J., Friedrichs, C. T., and Sanford, L. P.: Mud matrix solids fraction and bed erodibility in the York River
701 estuary, USA, and other muddy environments, Cont. Shelf Res., 31, (10, Supplement), S3-S13,
702 doi:10.1016/j.csr.2010.02.008, 2011.

703 DiToro, D. M.: Sediment Flux Modeling, Wiley-Interscience, New York, 624 pp, 2001.

704 Ditschke, D. and Markofsky, M.: A time-dependent flocculation model, in: Kusuda, T., Yamanishi, H., Spearman, J.,
705 Gailani, J. Z. (Eds.) Sediment and Ecohydraulics - INTERCOH 2005, Proceedings in Marine Science, 9,Elsevier,
706 Amsterdam, 241–253, doi:10.1016/S1568-2692(08)80019-8, 2008.

707 Droppo, I. G., Leppard, G. G., Liss, S. N., and Milligan, T. G.: Opportunities, needs, and strategic direction for research on
708 flocculation in natural and engineered systems, in: Droppo, I. G., Leppard, G. G., Liss, S. N., and Milligan, T. G.,
709 (Eds.), Flocculation in Natural and Engineered Environmental Systems, CRC Press, London, 407–421, 2005.

710 Dyer, K. R.: Coastal and Estuarine Sediment Dynamics, John Wiley and Sons, Chichester, 1986.

711 Edmonds, D. A., and Slingerland, R. L.: Significant effect of sediment cohesion on delta morphology, Nat. Geosci., 3(2),
712 105–109, doi:10.1038/NGE0730, 2010.

713 Eisma, D.: Flocculation and de-flocculation of suspended matter in estuaries, Neth. J. Sea Res., 20, 2/3, 183–199, 1986.

714 Fall, K. A., Harris, C. K., Friedrichs, C. T., Rinehimer, J. P., and Sherwood, C. R.: Model behavior and sensitivity in an
715 application of the cohesive bed component of the Community Sediment Transport Modeling System for the York
716 River Estuary, VA, USA, J. Mar. Sci. Eng., 2, 413–436, doi:10.3390/jmse2020413, 2014.

717 Fasham, M. J. R., Ducklow, H. W., and McKelvie S. M.: A nitrogen-based model of plankton dynamics in the oceanic
718 mixed layer, J. Mar. Res., 48, 591-639, 1990.

719 Fennel, K., Wilkin, J., Levin, J., Moisan, J., and O'Reilly, J.: Nitrogen cycling in the Middle Atlantic Bight: Results from a
720 three-dimensional model and implications for the North Atlantic nitrogen budget, Global Biogeochem. Cycles, 20,
721 GB3007, 14, 2006.

722 Harris, C. K. and Wiberg, P. L.: Approaches to quantifying long-term continental shelf sediment transport with an example
723 from the northern California STRESS mid-shelf site, Cont. Shelf Res., 17, 1389–1418, 1997.

724 Harris, C. K. and Wiberg, P. L.: A two-dimensional, time-dependent model of suspended sediment transport and bed
725 reworking for continental shelves, Comput. Geosci., 27, 6, 675–690, 2001.

726 Hill, P. S.: Sectional and discrete representations of floc breakage in agitated suspensions, Deep-Sea Res. PT I, 43, 5, 679–
727 702, 1996.

728 Hill, P. S. and Nowell, A. R. M.: Comparison of two models of aggregation in continental-shelf bottom boundary layers, J.
729 Geophys. Res., 100, C11, 22,749–22,763, 1995.

730 Hirano, M.: River bed degradation with armouring, in: Proceedings, Japan Society of Civil Engineers, Vol. 195, Japan, 1971.

731 HydroQual, Inc.: A Primer for ECOMSED Version 1.4 Users Manual, HydroQual, Inc., Mahwah, NJ, 2004.

732 Jacobs, W., Le Hir, P., Van Kesteren, W., and Cann, P.: Erosion threshold of sand - mud mixtures, Cont. Shelf Res., 31, 10
733 Supplement, S14–S25, doi:10.1016/j.csr.2010.05.012, 2011.

734 Keyvani, A. and Strom, K.: Influence of Cycles of High and Low Turbulent Shear on the Growth Rate and Equilibrium Size
735 of Mud Flocs, Mar. Geol., 354, 1–14, doi:10.1016/j.margeo.2014.04.010, 2014.

736 Khelifa, A. and Hill, P. S.: Models for effective density and settling velocity of flocs. J. Hydraul. Res., 44, 3, 390–401, 2006.

737 Knoch, D. and Malcherek, A.: A numerical model for simulation of fluid mud with different rheological behaviors, Ocean
738 Dyn., 61, 245–256, doi: 10.1007/s10236-010-0327-x, 2011.

739 Kranenburg, C.: The fractal structure of cohesive sediment aggregates, Estuar. Coast. Shelf Sci., 39, 451–460, 1994.

740 Krone, R. B.: Flume studies of the transport of sediment in estuarial shoaling processes, Final Report, Hydraulic Engineering
741 Laboratory and Sanitary Engineering Research Laboratory, Univ. of California, Berkeley, 1962.

742 Krone, R. B.: A study of rheologic properties of estuarial sediments, Technical Bulletin 7, Vicksburg, MS., U.S. Army Corps
743 of Engineers Communication on Tidal Hydrodynamics, 1963.

744 Le Hir, P., Cayocca, F., and Waeles, B.: Dynamics of sand and mud mixtures: A multiprocess-based modelling strategy,
745 Cont. Shelf Res., 3, 10 Supplement, S135–S149, 2011.

746 Lecroart, P., Maire, O., Schmidt, S., Grémare, A., Anschutz, P., and Meysman F. J. R.: Bioturbation, short-lived
747 radioisotopes, and the tracer-dependence of biodiffusion coefficients, Geochim. Cosmochim. Ac., 74, 21, 6049–
748 6063, doi:10.1016/j.gca.2010.06.010, 2010.

749 Letter, J. V.: Significance of probabilistic parameterization in cohesive sediment bed exchange, Ph.D. Thesis, Univ. of
750 Florida, Gainesville, 2009.

751 Letter, J. V. and Mehta, A. J.: A heuristic examination of cohesive sediment bed exchange in turbulent flows, Coast. Eng.,
752 58, 779–789, 2011.

753 Li, Q. W., Benson M. Harlan, M., Robichaux, P., Sha, X., Xu, K., and Straub, K. M.: Influence of sediment cohesion on
754 deltaic morphodynamics and stratigraphy over basin-filling time scales. J. Geophys. Res. Earth Surf. 2017JF004216
755 doi:10.1002/2017JF004216, 2017.

756 Lick, W., Huang, H., and Jepsen, R.: Flocculation of fine-grained sediment due to differential settling, J. Geophys. Res., 98,
757 10279–10288, 1993.

758 Lumborg, U. and Windelin, A.: Hydrography and cohesive sediment modelling: application to the Romo Dyb tidal area, J.
759 Mar. Syst., 38, 3-4, 287–303, 2003.

760 Lumborg, U.: Modelling the deposition, erosion, and flux of cohesive sediment through Oresund, J. Mar. Syst., 56, 1-2,
761 179–193, 2005.

762 Lumborg, U. and Pejrup, M.: Modelling of cohesive sediment transport in a tidal lagoon--an annual budget, Mar. Geol., 218,
763 1-4, 1–16, 2005.

764 Maa, J. P.-Y., Sanford, L. P. and Schoellhamer, D. H. (Eds): Estuarine and Coastal Fine Sediment Dynamics: INTERCOH
765 2003, vol 8, Proceedings in Marine Science, Elsevier, Amsterdam, 2007.

766 MacCready, P., and Geyer, W. R.: Estuarine salt flux through an isohaline surface, J. Geophys. Res., 106, 11629–11637,
767 2001.

768 MacDonald, I., Vincent, C. E., Thorne, P. D., and Moate, B. D.: Acoustic scattering from a suspension of flocculated
769 sediments, J. Geophys. Res.,118, 2581–2594, doi:10.1002/jgrc.20197, 2013.

770 Manning, A. J., Dyer, K. R.: Mass settling flux of fine sediments in Northern European estuaries: measurements and
771 predictions. Marine Geology 245, 107–122, 2007.

772 McAnally, W. H.: Aggregation and Deposition of Estuarial Fine Sediment, Ph.D. Thesis, Univ. of Florida, 382 pp, 1999.

773 McAnally, W. H. and Mehta, A. J.: Collisional aggregation of fine estuarial sediment, in: McAnally, W. H. and Mehta, A. J.
774 (Eds.), Coastal and Estuarine Fine Sediment Processes, Elsevier, 19-39, 2001.

775 McCave, I. N. and Swift, S. A.: A physical model for the deposition of fine-grained sediments in the deep sea, Bull. Geol.
776 Soc. Am., 87, 541–546, 1976.

777 McCave, I. N.: Size spectra and aggregation of suspended particles in the deep ocean, Deep-Sea Res., 31, 4, 329–352, 1984.

778 Mehta, A. J.: Characterization of cohesive sediment properties and transport processes in estuaries, in: Mehta, A. J. (Ed.)
779 Lecture Notes on Coastal and Estuarine Studies, Vol 14, Springer, Berlin, 290–325, 1986.

780 Mehta, A. J.: An Introduction to the Hydraulics of Fine Sediment Transport, World Scientific, 1039 pp, 2014.

781 Merkel, U. H. and Kopmann, R.: A continuous vertical grain sorting model for Telemac & Sisyphe, in: Munoz, R. M. (Ed)
782 River Flow 2012, Taylor & Francis, London, 2012.

783 Mitchener, H. and Torfs, H.: Erosion of mud/sand mixtures, Coast. Eng., 29, 1-2, 1–25, 1996.

784 Moriarty, J.M., Harris, C.K., Fennel, K., Friedrichs, M.A.M., Xu, K,, and Rabouille, C.: The roles of resuspension, diffusion
785 and biogeochemical processes on oxygen dynamics offshore of the Rhône River, France: a numerical modeling
786 study. Biogeosciences 14, 1919-1946, 2017.

787 Nguyen, H.-H. and Chua, L. H. C.: Simplified physically based model for estimating effective floc density, J. Hydraul. Eng.,
788 137, 8, 843–846, 2011.

789 Panagiotopoulos, I., Voulgaris, G., and Collins, M. B.: The influence of clay on the threshold of movement in fine sandy
790 beds, Coast. Eng., 32, 19–43, 1997.

791 Ralston, D. K., Geyer, W. R. and Warner, J. C.: Bathymetric controls on sediment transport in the Hudson River estuary:
792 Lateral asymmetry and frontal trapping, J. Geophys. Res. 117, C10013, 2012.

793 Rinehimer, J. P., Harris, C. K., Sherwood, C. R., and Sanford, L. P.: Sediment consolidation in a muddy, tidally-dominated
794 environment: Model behavior and sensitivity, Estuarine and Coastal Modeling, Proceedings of the Tenth
795 International Conference: 819–838, 2008.

796 Sanford, L. P. and Maa, J. P. Y.: A unified erosion formulation for fine sediments, Mar. Geol., 179(1-2), 9–23, 2001.

797 Sanford, L. P.: Modeling a dynamically varying mixed sediment bed with erosion, deposition, bioturbation, consolidation,
798 and armoring, Comput. Geosci., 34, 1263–1283, 2008.

799 Shchepetkin, A. F. and McWilliams, J. C.: The Regional Oceanic Modeling System (ROMS): A Split-Explicit, Free-Surface,
800 Topography-Following-Coordinate Oceanic Model, Ocean Model., 9, 4, 347–404,
801 doi:10.1016/j.ocemod.2004.08.002, 2005.

802 Sherwood, C. R., Drake, D. E., Wiberg, P. L., and Wheatcroft, R. A.: Prediction of the fate of p,p'-DDE in sediment on the
803 Palos Verdes shelf, California, USA, Cont. Shelf Res., 22, 6-7, 1025–1058, 2002.

804 Slade, W. H., Boss, E. S., and Russo, C.: Effects of particle aggregation and disaggregation on their inherent optical
805 properties, Opt. Express, 19, 9, 7945–7959, 2011.

806 Smoluchowski, M.: Versuch einer mathematischen theorie des koagulations-kinetik kolloid losungren, Zeitschrift fur
807 Physikalische Chemie, 92, 129–168, 1917.

808 Soulsby, R. L., Manning, A. J., Spearman, J., and Whitehouse, R. J. S.: Settling Velocity and Mass Settling Flux of
809 Flocculated Estuarine Sediments, Mar. Geol., 339, 1–12, doi:10.1016/j.margeo.2013.04.006, 2013.

810 Spearman, J. R., Manning, A. J., and Whitehouse, R. J. S.: The settling dynamics of flocculating mud and sand mixtures:
811 part 2—numerical modelling. Ocean Dyn., 61, 351–370, 2011.

812 Stone, M., Krishnappan, B. G., and Emelko, M. B.; The effect of bed age and shear stress on the particle morphology of
813 eroded cohesive river sediment in an annular flume, Water Res., 42, 15, 4179–4187, doi:
814 10.1016/j.watres.2008.06.019, 2008.

815 Swift, D. J. P., Stull, J. K., Niedoroda, A. W., Reed, C. W., Wong, G. T. F., and Foyle, B. A.: Estimates of the Biodiffusion
816 Coefficient, DB, from Composition of the Benthic Infaunal Community, Report prepared for the Los Angeles
817 County Sanitation Districts, Contribution No. 5 of the Sediment Dynamics Laboratory, Old Dominion University,
818 Norfolk, Virginia, 1994.

819 Swift, D. J. P., Stull, J. K., Niedoroda, A. W., Reed, C. W., and Wong, G. T. F.: Contaminant dispersal on the Palos Verdes
820 continental margin: II. Estimates of biodiffusion coefficient, Db, from composition of the benthic infaunal
821 community, Sci. Total Environ., 179, 91–107, 1996.

822 Tambo, N. and Watanabe, Y.; Physical characteristics of flocs. I The floc density function and aluminium floc. Water
823 Research 13, 409–419, 1979.

824 Tassi, P. and Villaret, C.: SISYPHE v6.3 User's Manual, EDF, Laboratoire National d'Hydrulique et Environnement,
825 Chatou, France, 73 pp, 2014.

826 Thorne, P. D., MacDonald, I. T., and Vincent, C. E.: Modelling acoustic scattering by suspended flocculating sediments,
827 Cont. Shelf Res., 88, 81–91, doi:10.1016/j.csr.2014.07003, 2014.

828 Umlauf, L. and Burchard, H.: A generic length-scale equation for geophysical turbulence models, J. Mar. Res., 61, 2, 235–
829 265, 2002.

van Leussen, W.: Estuarine macroflocs and their role in fine-grained sediment transport, Ph.D. Thesis, University of Utrecht, Utrecht, The Netherlands, 1994.

van Ledden, M., van Kesteren, W. G. M., and Winterwerp, J. C.: A conceptual framework for the erosion behaviour of sand - mud mixtures, Cont. Shelf Res., 24, 1, 1–11. doi:10.1016/j.csr.2003.09.002, 2004.

van der Wegen, M., Dastgheib, A., Jaffe, B. E., and Roelvink, D.: Bed composition generation for morphodynamic modeling: case study of San Pablo Bay in California, USA, Ocean Dyn., 61, 173–186, doi:10.1007/s10236-010-0314-2, 2011.

Verney, R., Lafite, R., Brun-Cottan, J. C., and Le Hir, P.: Behaviour of a floc population during a tidal cycle: Laboratory experiments and numerical modeling, Cont. Shelf Res., 31, S64–S83, doi:10.1016/j.csr.2010.02.005, 2011.

Villaret, C., Hervouet, J.-M., Kopmann, R., Merkel, U., and Davies, A. G.: Morphodynamic modeling using the Telemac finite-element system, Comput. Geosci., 53, 105–113, doi:10.1016/j.cageo.2011.10.004, 2011.

Warner, J. C., Armstrong, B., He, R., and Zambon, J. B.: Development of a coupled ocean-atmosphere-wave-sediment transport (COAWST) modeling system, Ocean Model., 35, 230–244, doi:10.1016/j.ocemod.2010.07.010, 2010.

Warner, J. C., Sherwood, C. R., Arango, H. G., and Signell, R. P.: Performance of four turbulence closure models implemented using a generic length scale method, Ocean Model., 8, 1/2, 81–113, doi:10.1029/2004JC002691, 2005.

Warner, J. C., Sherwood, C. R., Signell, R. P., Harris, C. K., and Arango, H. G.: Development of a three-dimensional, regional, coupled wave, current, and sediment-transport model, Comput. Geosci., 34, 1284–1306, 2008.

Wheatcroft, R. A. and Martin, W. R.: Spatial variation in short-term (^{234}Th) sediment bioturbation intensity along an organic-carbon gradient, J. Mar. Res., 54, 763–792, 1996.

Whitehouse, R. J. S., Soulsby, R. L., Roberts, W., and Mitchener, H.: Dynamics of Marine Muds, Thomas Telford, London, 2000.

Wiberg, P. L., Drake, D. E., and Cacchione, D. A.: Sediment resuspension and bed armoring during high bottom stress events on the northern California inner continental shelf: measurements and predictions, Cont. Shelf Res.,14, 10/11, 1191–1219, 1994.

Winterwerp, J. C.: On the Dynamics of High-Concentrated Mud Suspensions, Technical University of Delft, Delft, The Netherlands, 1999.

857 Winterwerp, J. C.: On the flocculation and settling velocity of estuarine mud, Cont. Shelf Res., 22, 9, 1339–1360, 2002.

858 Winterwerp, J. C., Bale, A. J., Christie, M. C., Dyer, K. R., Jones, S., Lintern, D. G., Manning, A. J., Roberts, W., and
859 Kranenburg, C.: Flocculation and settling velocity of fine sediment. In: Proceedings in Marine Science, Vol. 5,
860 Elsevier, 25–40, 2002

861 Winterwerp, J. C. and Kranenburg, C. (Eds.): Fine Sediment Dynamics in the Marine Environment, Proceedings in Marine
862 Science, Vol 5, Elsevier, Amsterdam, 2002.

863 Winterwerp, J. C., Maa, J. P.-Y., Sanford, L. P., and Schoellhamer, D. H.: On the sedimentation rate of cohesive sediment,
864 in: Proceedings in Marine Science, 8, Elsevier, 209–226, 2007

865 Winterwerp, J. C., Manning, A. J., Martens, C., de Mulder, T., and Vanlede J.: A heuristic formula for turbulence-induced
866 flocculation of cohesive sediment, Estuar. Coast. Shelf Sci., 68, 1-2, 195–207, 2006.

867 Winterwerp, J. C. and van Kesteren, W. G. M.: Introduction to the Physics of Cohesive Sediment in the Marine
868 Environment, Elsevier, Amsterdam, 2004.

869 Xu, F., Wang, D.-P., and Riemer, N.: Modeling flocculation processes of fine-grained particles using a size-resolved
870 method: Comparison with published laboratory experiments, Cont. Shelf Res., 28, 2668–2677.
871 doi:10.1016/j.csr.2008.09.001, 2008.

872 Xu, F., Wang, D.-P., and Riemer, N.: An idealized model study of flocculation on sediment trapping in an estuary turbidity
873 maximum, Cont. Shelf Res., 30, 1314–1323. doi:10.1016/j.csr.2010.04.014, 2010.

874

875

Geosci. Model Dev. Discuss., https://doi.org/10.5194/gmd-2017-267
Manuscript under review for journal Geosci. Model Dev.
Discussion started: 1 December 2017

Geoscientific Model Development Discussions

876 **Table**

877
878 **Table 1. Characteristics of the estuary turbidity maxima for seven cases under different flocculation conditions.**

Case	0	1	2	3	4	5	6
	No flocs	α = 0.35 β = 0.15 no defloc	α = 0.35 β = 0.15 defloc=5h	α = 0.35 β = 0.15 defloc=50h	α = 0.45 β = 0.10 defloc=50h	α = 0.25 β = 0.20 defloc=50h	α = 0.35 β = 0.34 defloc=50h
Mean SSC @ maximum (kg/m^3)	1.23	0.46	0.45	0.45	0.45	0.46	0.46
Maximum SSC (kg/m^3)	3.1	3.6	3.7	3.7	4.1	3.2	2.9
D_{50} at SSC maximum (μm)	37	539	529	529	622	426	384
D_{50} at SSC maximum; 12-h mean (μm)	37	255	249	250	325	181	167
w_s at SSC maximum (mm/s)	0.13	1.91	1.87	1.87	2.2	1.51	1.36
w_s at SSC maximum; 12-h mean (mm/s)	0.13	0.90	0.88	0.89	1.15	0.64	0.59
Locus of maximum deposition (km from ocean boundary)	80 ± 30	19 ± 11	18 ± 10	18 ± 11	19 ± 10	79 ± 69	16 ± 6
Maximum deposit thickness (mm)	4.2 ± 5.8	31.6 ± 12.8	25.8 ± 10.1	26.1 ± 10.4	27.1 ± 10.9	5 ± 10.1	25 ± 10.2
Maximum deposit D_{50} (μm)	18.5 ± 0	218 ± 87.1	40.9 ± 71.3	75.5 ± 76.1	92.9 ± 94.2	69.5 ± 89.9	25.4 ± 40.4

879

Geosci. Model Dev. Discuss., https://doi.org/10.5194/gmd-2017-267
Manuscript under review for journal Geosci. Model Dev.
Discussion started: 1 December 2017

Geoscientific Model Development Discussions

880 **Figures**

881

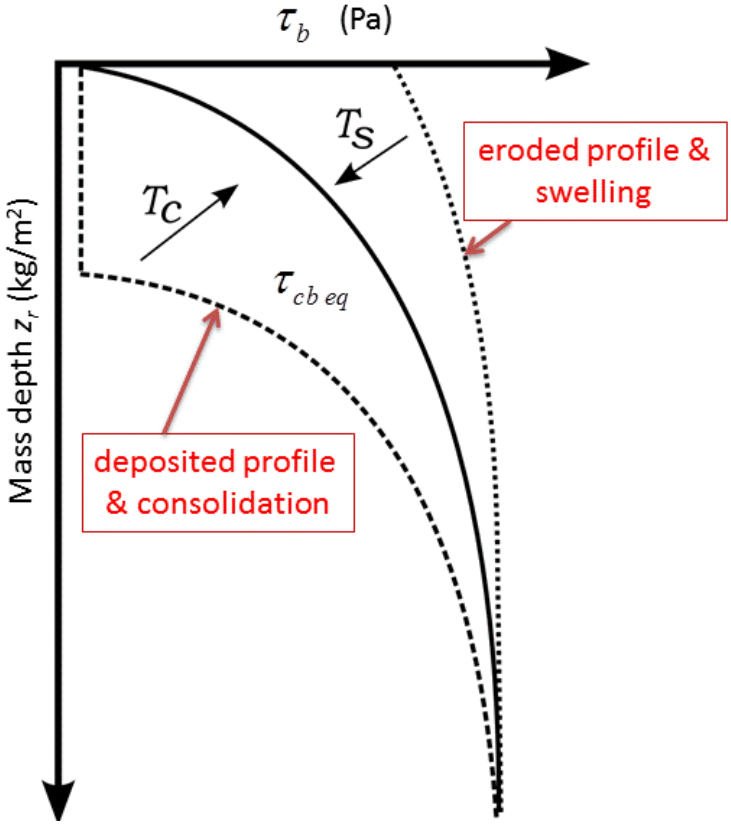

Figure 1. Conceptual diagram of consolidation and swelling (Rinehimer et al., 2008). The equilibrium bulk critical stress for erosion profile, $\tau_{cbeq}(z)$ is shown as the solid line. The dotted line represents a critical shear stress profile following sediment erosion. The dashed line is a profile after deposition of sediment with a low τ_c at the surface. The arrows indicate consolidation and swelling toward the equilibrium profile with the timescales T_c and T_s, respectively.

882

883

Geosci. Model Dev. Discuss., https://doi.org/10.5194/gmd-2017-267
Manuscript under review for journal Geosci. Model Dev.
Discussion started: 1 December 2017

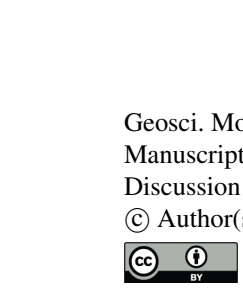

Geoscientific Model Development Discussions

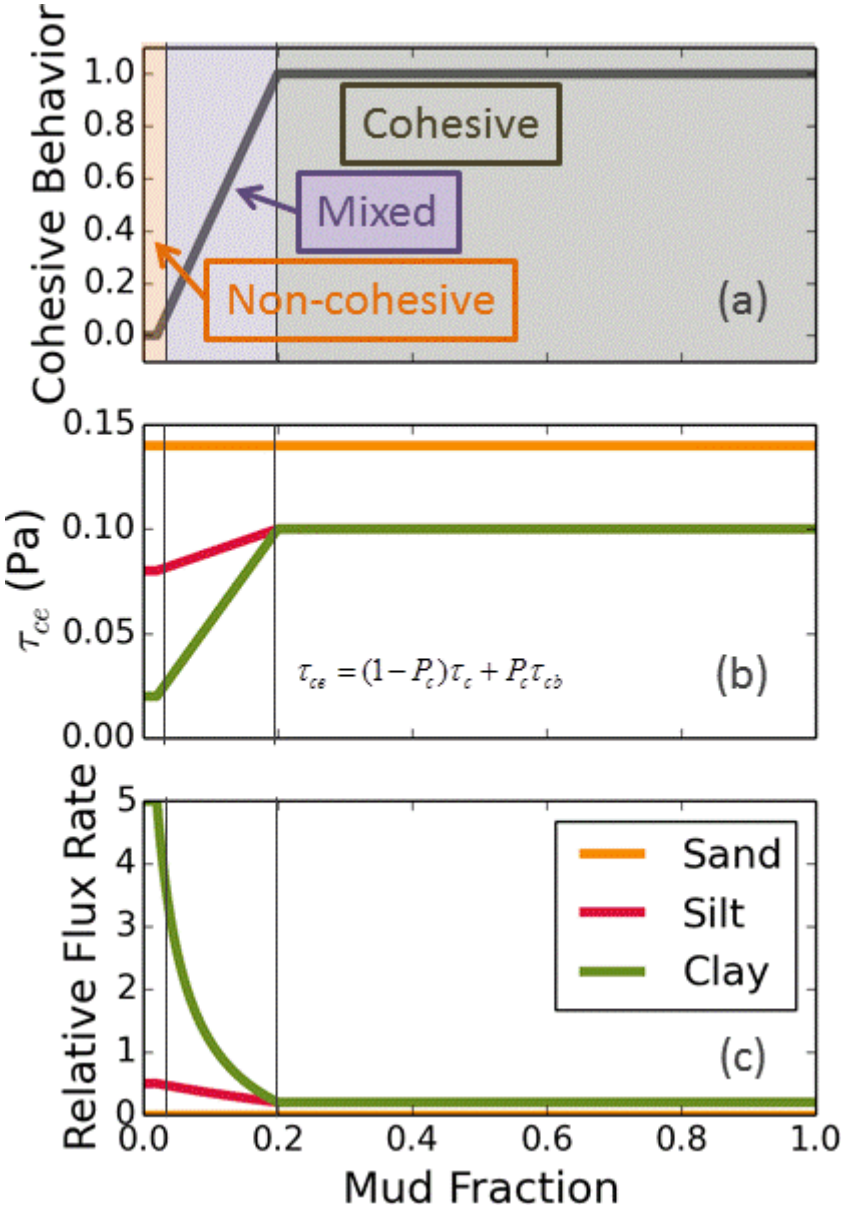

Figure 2. Summary of mixed-bed behavior with increasing of mud fraction f_c (the combined mass fraction of material in cohesive classes). (a) Cohesive behavior parameter P_c as a function of f_c. (b) Effective critical shear stress τ_{ce} for size classes where bulk critical shear stress of the bed τ_{cb} = 0.1 Pa . (c) Relative flux (normalized excess shear stress) from the bed when bed stresses are ~τ_b = 0.12 Pa (greater than τ_c for clay and silt primary particles, but less than τ_c for sand)

Geosci. Model Dev. Discuss., https://doi.org/10.5194/gmd-2017-267
Manuscript under review for journal Geosci. Model Dev.
Discussion started: 1 December 2017

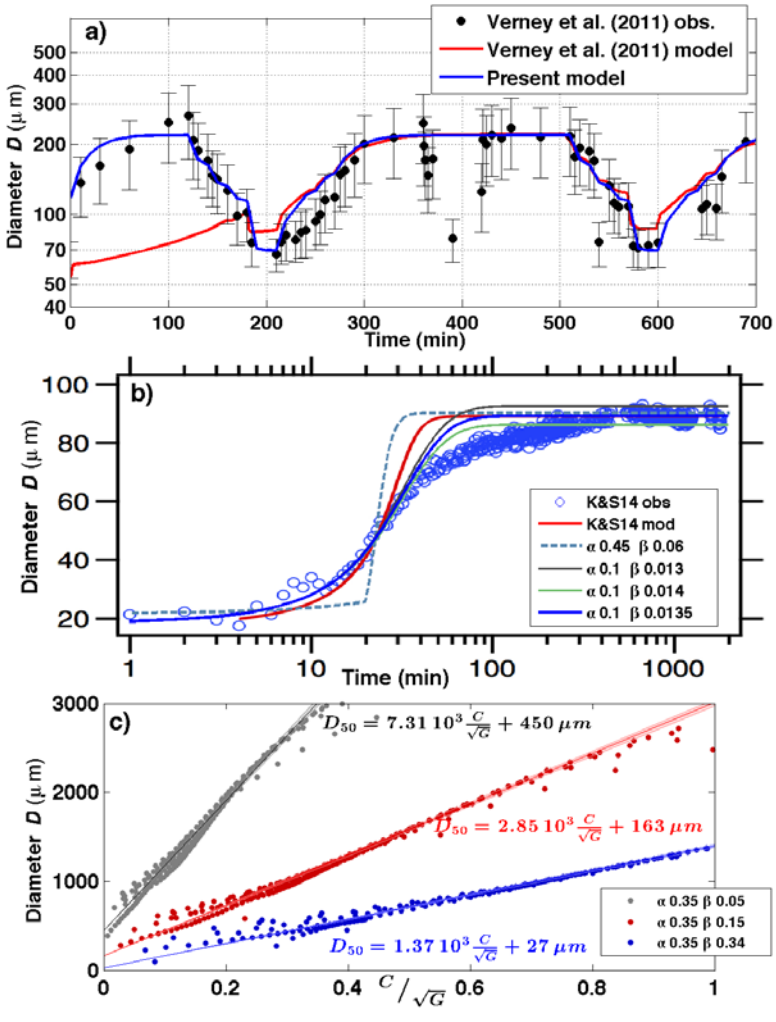

Figure 3. Comparison of ROMS implementation of FLOCMOD with laboratory and theoretical results. (a) Laboratory response of floc size to simulated fluctuations in shear rate *G* showing observed area-weighted floc diameter *D* (black dots with error bars), model results presented in Verney et al., (2011; red line), and ROMS FLOCMOD simulation (blue line). (b) Laboratory response of floc size to rapid increase in shear rate from *G*=0 to *G*=15 s^{-1} showing sizes measured by Keyvani and Strom (2014; K&S14; blue circles), K&S14 model results (red line), and ROMS FLOCMOD results for various combinations of aggregation and breakup parameters (dashed and colored lines). (c) Equilibrium diameters produced by steady ROMS FLOCMOD simulations with a range of concentrations, shear rates, and aggregation and breakup parameters (dots). These fall along lines with slopes determined by the ratio of aggregation and breakup parameters, according to theory (Winterwerp, 1998).

Geosci. Model Dev. Discuss., https://doi.org/10.5194/gmd-2017-267
Manuscript under review for journal Geosci. Model Dev.
Discussion started: 1 December 2017

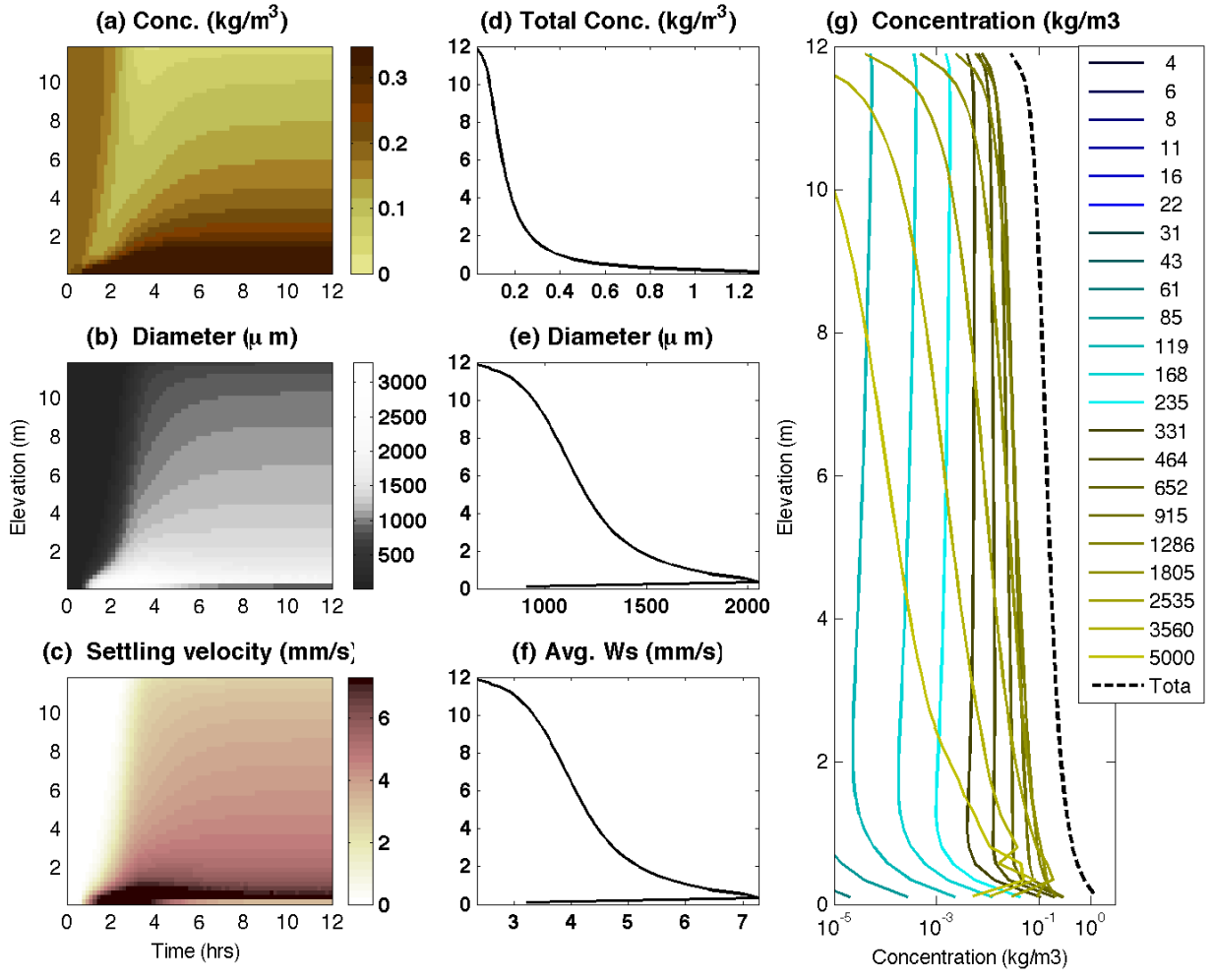

Figure 4. Simulation of steady open-channel flow initialized with a vertically uniform concentration of 0.2 kg/m^3 in the 8-μm class. Temporal evolution of profiles of (a) mass concentration (b) mass-weighted diameter (c) mass-weighted settling velocity. Final profiles of (d) concentration, (e) diameter and (f) settling velocity, and (g) final concentration profiles for each class size (colored lines) and sum of all classes (dashed line).

Geosci. Model Dev. Discuss., https://doi.org/10.5194/gmd-2017-267
Manuscript under review for journal Geosci. Model Dev.
Discussion started: 1 December 2017

Geoscientific Model Development Discussions

889

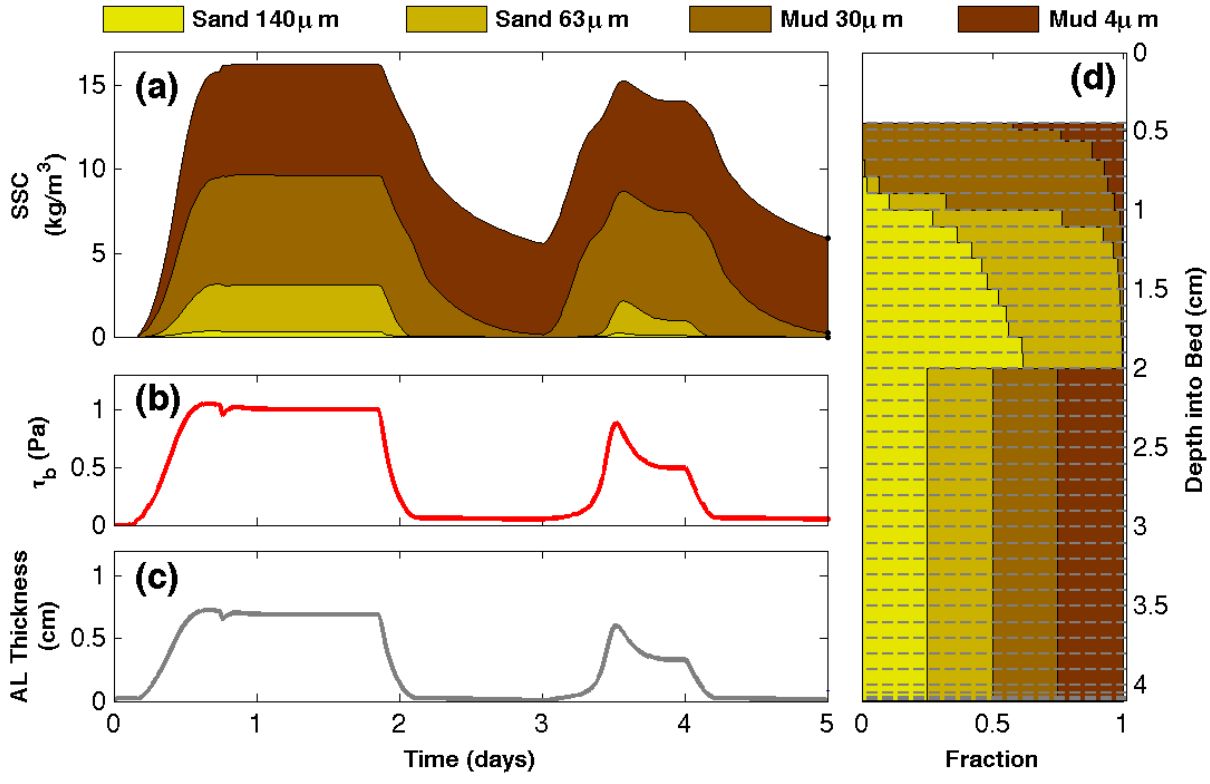

Figure 5. Summary of the double resuspension experiment with non-cohesive sediment over 5 days. The model setup included 41 bed layers, a minimum new layer thickness of 1 mm, and four non-cohesive classes. The top horizontal panel (a) shows the time evolution of the mass of sediment in suspension, colored by size class. The middle horizontal panel (b) is the time series of bottom stress, and the bottom horizontal panel (c) shows the corresponding time series of active-layer thickness. The right panel (d) depicts the final stratigraphy relative to the initial bed level at zero and shows the fraction of each sediment class in each bed layer.

890

Geosci. Model Dev. Discuss., https://doi.org/10.5194/gmd-2017-267
Manuscript under review for journal Geosci. Model Dev.
Discussion started: 1 December 2017

891

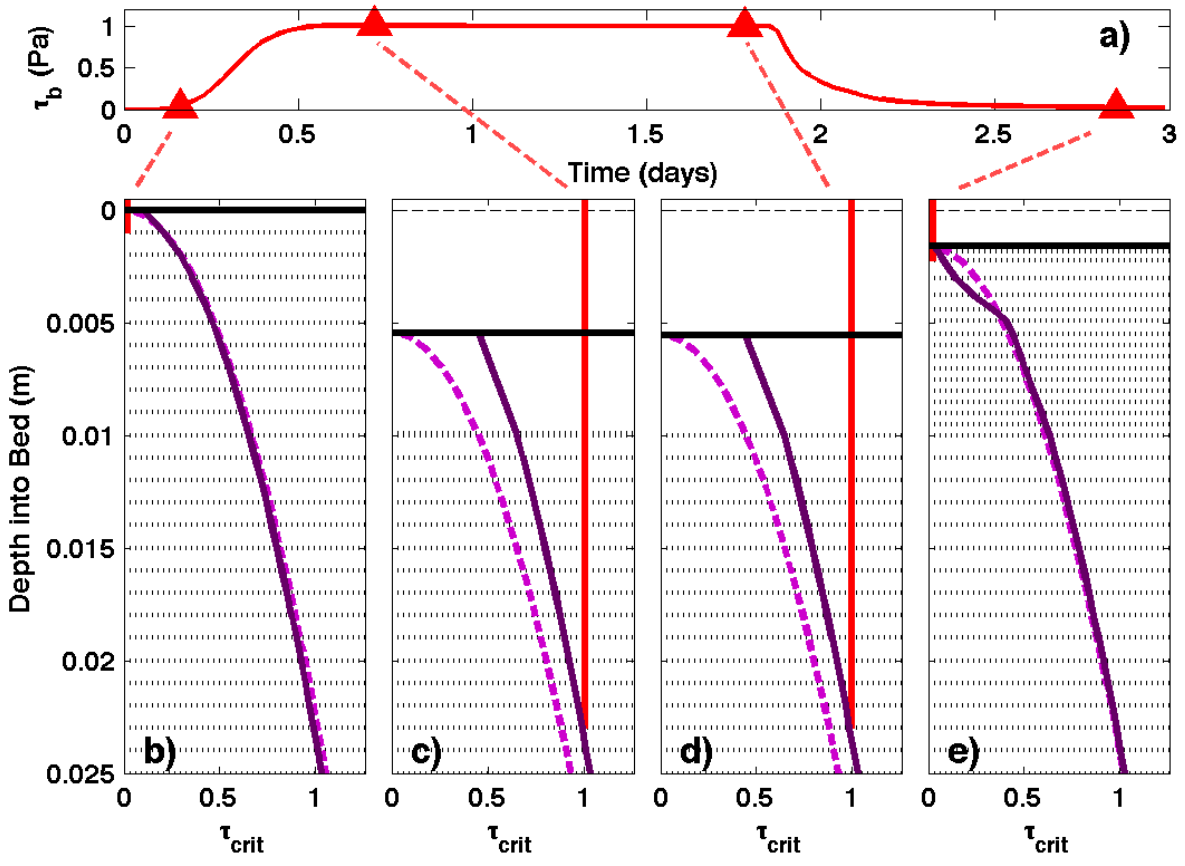

Figure 6. Time series of bottom stress (a) and profiles of critical shear stress for erosion during four distinct conditions: (b) initial bed condition; (c) eroded bed (after 0.7 days with τ_b= 1.0 Pa); (d) unchanged bed level but modified bulk critical stress profile after 1.2 additional days with τ_b = 1.0 Pa); and (e) deposition after a day of low stress with τ_b =0.1 Pa). In the lower panels, the solid red line is the magnitude of the bottom stress (τ_b), the dashed magenta line is the equilibrium profile of bulk critical stress for erosion $\tau_{cb}(z)$, and the solid purple line is the instantaneous profile of bulk critical stress for erosion. The solid black line is the instantaneous position of the top of the bed at each time, with the initial bed elevation starting at zero.

892

Geosci. Model Dev. Discuss., https://doi.org/10.5194/gmd-2017-267
Manuscript under review for journal Geosci. Model Dev.
Discussion started: 1 December 2017

893

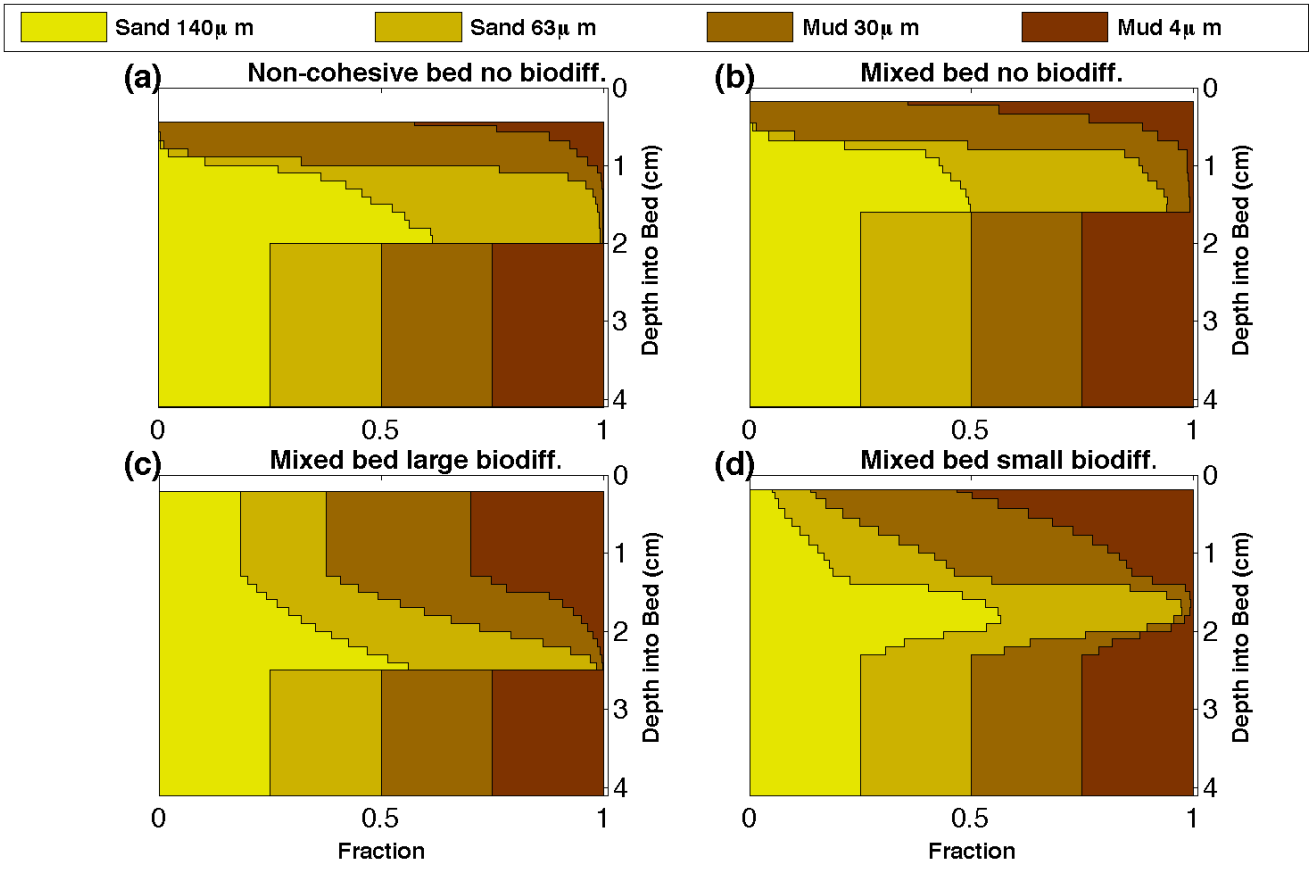

Figure 7. Comparison of final bed stratigraphy for resuspension and settling simulations showing the fraction of each sediment class distributed in each bed layer. (a) non-cohesive bed with no biodiffusion (same as Figure 5d, included for comparison); (b) mixed bed with no biodiffusion; (c) mixed bed with large biodiffusion (D_s=10^{-5} $m^2 s^{-1}$); and (d) mixed bed with small biodiffusion (D_s=10^{-10} $m^2 s^{-1}$). The final sediment fraction distribution after two successive erosion/deposition events lasting five days (similar to Figure 5b) is shown. The same four sediment classes were used in all experiments, but their cohesive behavior varied.

894

Geosci. Model Dev. Discuss., https://doi.org/10.5194/gmd-2017-267
Manuscript under review for journal Geosci. Model Dev.
Discussion started: 1 December 2017

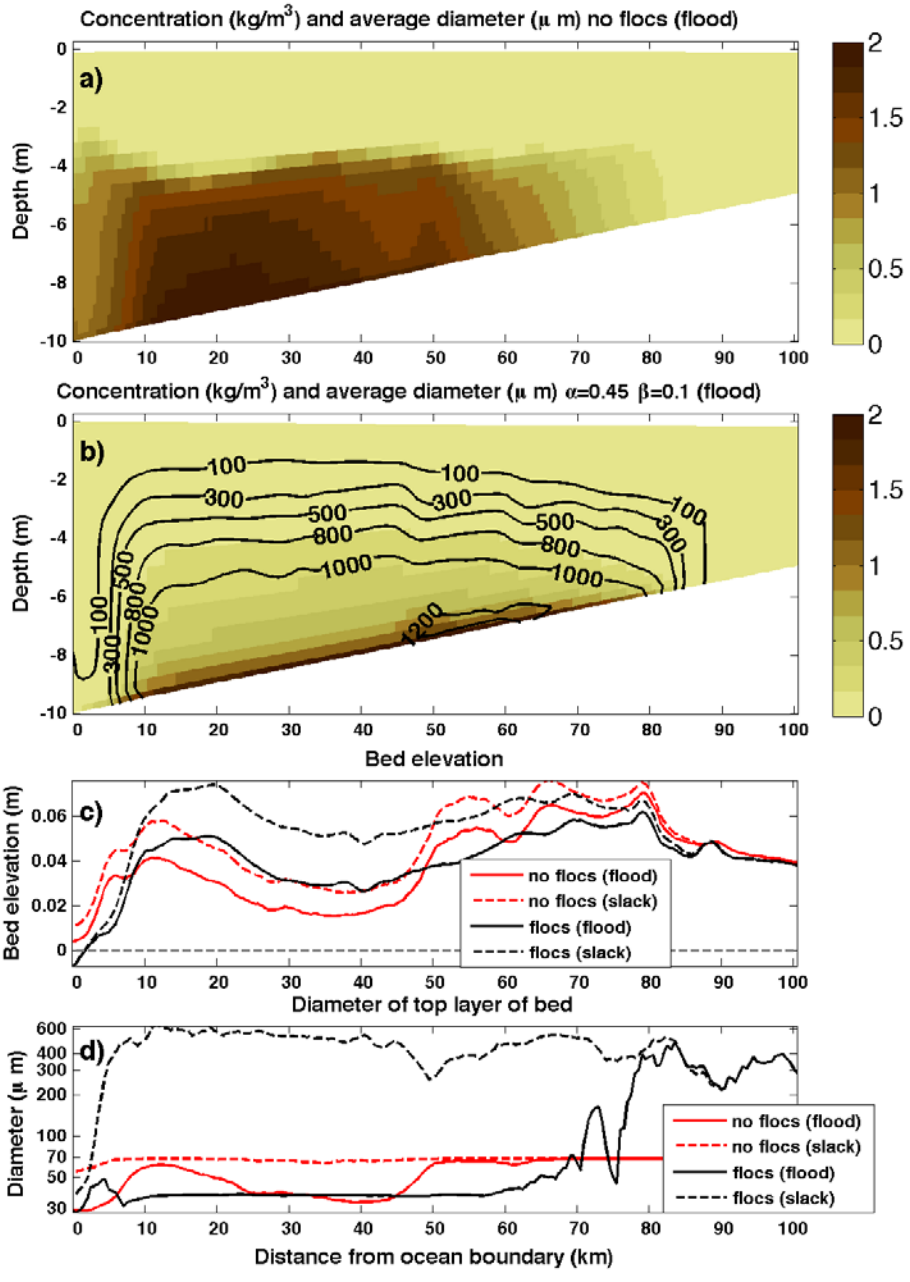

Figure 8. Comparison of estuarine turbidity maxima simulations with and without floc dynamics. The model was initialized with a uniform suspended-sediment concentration of 0.1 kg/m^3 in the 37-μm class.

Geosci. Model Dev. Discuss., https://doi.org/10.5194/gmd-2017-267
Manuscript under review for journal Geosci. Model Dev.
Discussion started: 1 December 2017

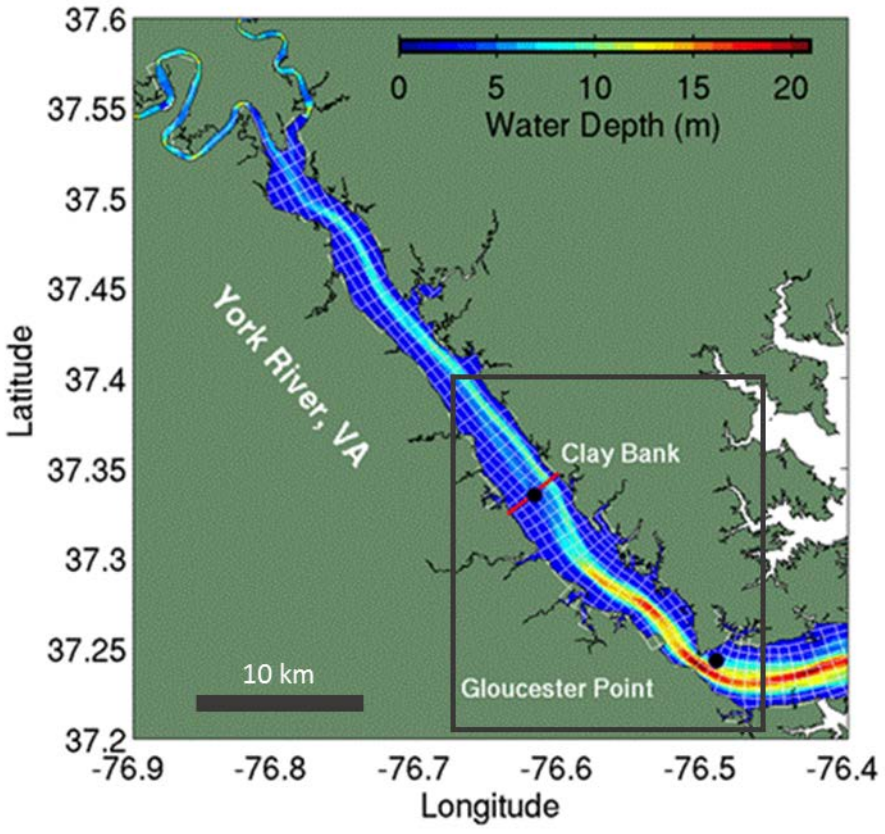

Figure 9. York River bathymetry (color scale), and model grid (white lines show every fifth grid line in the along- and across-channel directions). The region outlined in grey is expanded in Figure 10.

Geosci. Model Dev. Discuss., https://doi.org/10.5194/gmd-2017-267
Manuscript under review for journal Geosci. Model Dev.
Discussion started: 1 December 2017

Geoscientific Model Development Discussions
Open Access
EGU

898

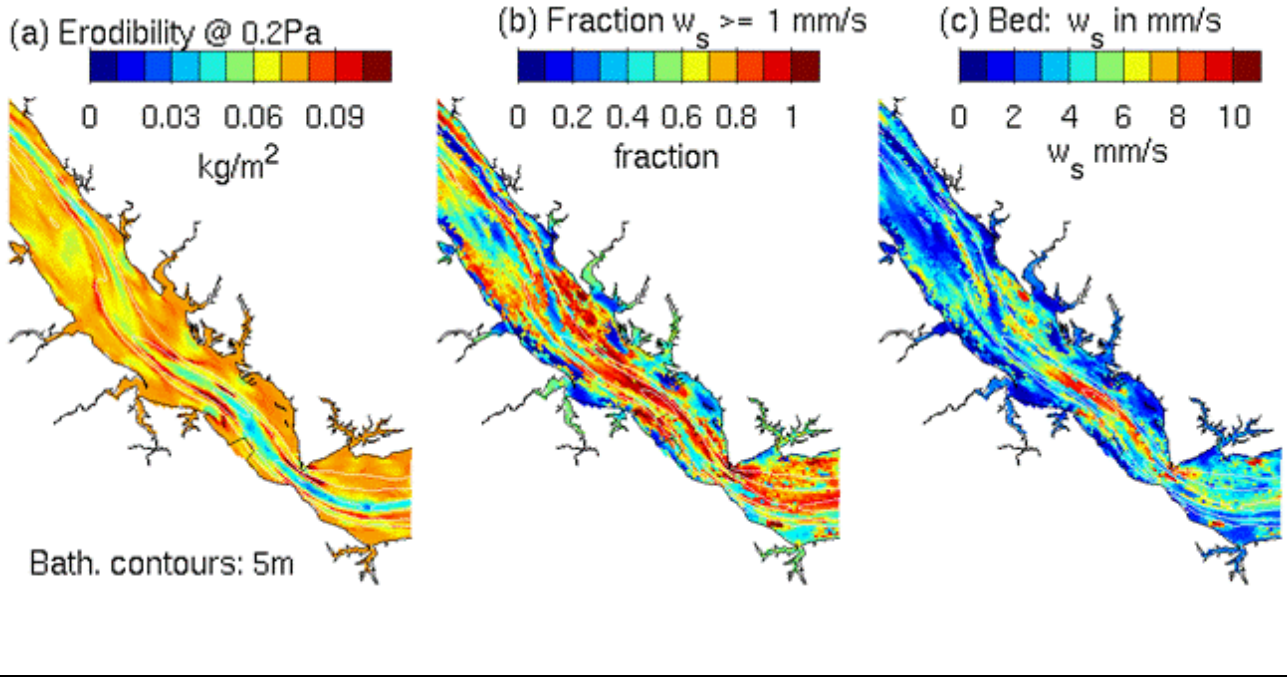

Figure 10. Model estimates of seabed properties after two months of tidal forcing and constant, average freshwater discharge. (a) Erodibility of the seabed, calculated as the thickness of the layer having a critical shear stress exceeded by 0.2 Pa. (b) Fraction of the surficial sediment in the "faster settling" size class. (c) Average settling velocity of surficial sediment.

899